

Synthesis of Magnetic Ferrite and TiO₂-Based Nanomaterials for Photocatalytic Water Splitting Applications



Wegdan Ramadan, Yamen AlSalka, Osama Al-Madanat, and Detlef W. Bahnemann

Abstract Clean non fossil sources of energy have an increasing urgency to support industrial and population growth to achieve this goal, the continuous development of nanostructures and nanomaterials for different applications such as photocatalytic water splitting is under intense investigation. Two of the most important materials namely, titanium dioxide, TiO₂, and ferrites having the MFe₂O₄ structure where M is transition metal are introduced in this chapter. Ferrites and titanium dioxide are two interesting nanostructures having great potential. Ferrites have many members in the family hence, offering diversity in structural and physical properties which in turn give chance for a large variety of purposes and applications. They own an energy band gap that is small enough to crop photons from the visible light region. They are also abundant on earth and have important physical properties like magnetism and multiferroicity in addition to being biocompatible which will increase their usability. On the other hand, TiO₂ has several advantages, including its stability in terms of chemical and thermal properties, in addition to its availability, photoactivity, and relatively elevated charge transfer ability. Furthermore, the nontoxicity, high oxidative strength, and cheap price are additional advantages. Despite the large band gap and its related UV-light activation, TiO₂ is one of the highly studied photocatalysts. Moreover, it has been extensively investigated in many aspects, including the kind

W. Ramadan (✉)

Faculty of Science, Physics Department, Alexandria University, Alexandria 21511, Egypt

e-mail: wegdan.ramadan@alexu.edu.eg

Y. AlSalka

Institut für Nanophotonik Göttingen e.V., Hans-Adolf-Krebs-Weg 1, 37077 Göttingen, Germany

O. Al-Madanat

Chemistry Department, Mutah University, Mutah, Al-Karak 61710, Jordan

D. W. Bahnemann

Institut Für Technische Chemie, Leibniz Universität Hannover, Callin Str. 3, 30167 Hannover, Germany

Laboratory “Photoactive Nanocomposite Materials”, Saint-Petersburg State University, Ulyanovskaya Str. 1, 198504 Saint-Petersburg, Russia

of the oxidative species ($\cdot\text{OH}$ radicals vs. h^+), the location of the photoinduced reactions (at the surface or in the bulk), and the ways that enhance the photocatalytic performance.. Many of the synthesis techniques for both, ferrites and TiO_2 were adopted to serve definite purposes like control over phase purity, morphology, size, and dispersion which are discussed in this chapter.

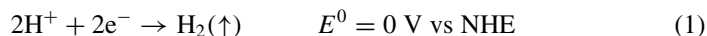
Keywords Ferrites · TiO_2 · Water splitting · Photocatalysis · Green hydrogen

1 Introduction

Fossil fuels were extensively exploited for decades to drive the development of our modern society without considering the potential damages to the sustainable environmental systems. Global energy consumption is projected to rise by 28% from 2015 to 2040 [48] with the simultaneous depletion of fossil fuels. Thus, the big global challenge is to fulfill the rising energy demand while minimizing environmental pollution. The quickest developing energy sources are anticipated to be renewables, having an annual increase in consumption of 2.3% from 2015 to 2040 [48]. The sun, which falls on the earth's surface with solar energy power of 1000 W m^{-2} , is indeed the largest and cleanest renewable energy resource [79, 96]. Solar energy is considered a sustainable energy supply when its transformation into chemical energy carriers is efficiently fulfilled.

Molecular Hydrogen owns the highest energy content, i.e., 120 MJ kg^{-1} , among other fuels [4, 11]. Therefore, H_2 can be considered a sustainable fuel when it is cleanly resulted from renewable or abundant origin at reasonable prices [126, 153]. Among other methods, solar hydrogen production seems to offer the best sustainable route. There are several processes to produce H_2 through water splitting reaction, including (1) thermochemical process using solar concentrators to split water via heat from concentrated sunlight [155], (2) photobiological process, in which aerobic or anaerobic Bacteria are used [42], (3) water electrolysis process, in which an external bias generated from renewable energy is applied for the electrically driven splitting of water [59], and (4) photocatalytic process, in which a suitable photocatalyst is suspended in an aqueous solution to convert the light energy into a chemical one [100].

The photocatalytic route for water splitting offers a sustainable conversion of energy from renewables in comparison with conventional processes based on electrolyzers [62]. This method has attracted attention due to the clean transformation of energies, i.e., light into chemical energy, using a photocatalytic material. Moreover, the ambient conditions are applied to carry out its two half-reactions (Eqs. 1, 2), in which protons are reduced to H_2 and water molecule is oxidized to O_2 through a 4-electron reaction, respectively [7, 14, 62]. The splitting of a water molecule is coupled with a change in ΔG^0 equal to 237.2 kJ/mol , i.e., $\Delta E^0 = 1.23 \text{ V}$ in compliance with the Nernst equation [165]. Thus, a photocatalytic system must absorb photon energy ($h\nu$) of at least 1.23 eV to thermodynamically split the water.

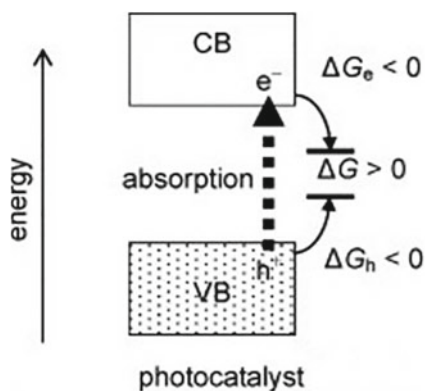


The overall water-splitting reaction has a $\Delta G > 0$, therefore, it absorbs energy. However, a suitable photocatalyst can indeed drive such a reaction with a positive ΔG value [128]. In contrast to a normal catalytic system, redox reactions are spatially separated using a photocatalyst, in which both ΔG_e and ΔG_h should be negative [129] as presented in Fig. 1. Accordingly, the thermodynamic demand water-splitting by photocatalysis is more cathodic energy level at the bottom of the CB compared with the standard electrode potential of (H^+/H_2) and more anodic energy level at the top of the valance band compared with the standard electrode potential of ($\text{O}_2/\text{H}_2\text{O}$), respectively [128, 135]. Therefore, only a few photocatalysts possess the thermodynamic driving force for the complete light induced splitting of water into H_2 and O_2 .

According to the previous thermodynamic discussion, photocatalysis is a process that includes photon absorption by material to induce a reaction that has enormously slow kinetics outside this system [62]. The so-called photocatalyst absorbs certain light energy during illumination and generates e^-/h^+ as charge carriers, which are the driving forces for the next redox reactions on the surface. The thus light-absorbing material is called photocatalyst, which, in heterogeneous systems, is usually semiconducting material [62]. Consequently, heterogeneous photocatalysis essentially relies on the unique properties of the semiconducting material for an efficient harvesting of incident light and successively initiate surface reactions.

Figure 1 illustrates a typical schematic of the significant steps involved during photocatalytic water-splitting. First (1), photogeneration of electron–hole pairs via suitable irradiation of a photocatalyst to excite electrons from the valence band (VB) to the conduction band (CB). Second (2), Separation and migration of charge carriers to reach the surface. Finally (3), the electrons on the photocatalyst or the co-catalyst participate in a reduction reaction and generate hydrogen, while the holes are involved

Fig. 1 Scheme of Gibbs-energy difference during photocatalytic reactions, reprinted with permission from Elsevier [128]



in an oxidation reaction to form oxygen or to oxidize an organic substrate. The criterion for an efficient photocatalyst is the solar–hydrogen conversion efficiency (STH) shown in Eqs. (3) [38]:

$$\eta_{\text{STH}} = \eta_{\text{A}} \times \eta_{\text{CS}} \times \eta_{\text{CT}} \times \eta_{\text{CR}} \quad (3)$$

The STH conversion efficiency depends on the capacity of light absorption (η_{A}), charge separation (η_{CS}), charge transportation (η_{CT}), and reaction efficiency (η_{CR}) (Fig. 2).

As an alternative, the so-called photocatalytic reforming is a process that brings together two photocatalytic processes, namely the split of water and the oxidation of organics [7]. An organic substrate can be oxidized at the photocatalyst surface instead of O_2 production, while protons can be reduced to H_2 by photogenerated electrons [12]. The thus organic substrate is frequently named sacrificial reagent due to its irreversible reaction with the photogenerated holes, prohibiting, consequently, the undesired e^-/h^+ recombination [15]. Because organics are commonly greater reducing agents than water, they can be oxidized at a less positive potential. Therefore, photocatalytic reforming can more easily meet the band edge potentials of a semiconductor than the overall photocatalytic water-splitting, offering more variety of suitable materials. In such systems, O_2 is not simultaneously produced, which inhibits the back reaction forming water from O_2 and H_2 , and avoids a gas separation stage [55]. A widespread range of organic substrates including alcohols and organic acids have been utilized as sacrificial reagents for H_2 evolution through photocatalysis [69].

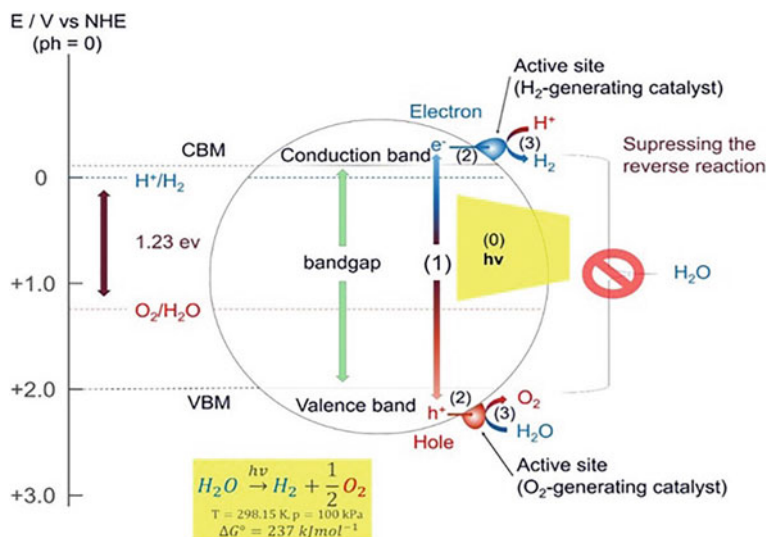


Fig. 2 The main steps of photocatalytic water-splitting on a semiconductor. Reproduced with permission Elsevier [120]

In this chapter, we concentrate primarily on the synthesis of two of the most important photocatalytic materials namely, TiO₂ and the ferrites family. They offer a lot of advantages to the field of photocatalysis in terms of their availability, stability, and response to light whether it is UV or visible. In particular, we focus on their application, performances, and the observed drawbacks in solar water-splitting. The progress witnessed in the field of materials science has been quite spectacular and this has enabled and fueled deep investigations on discovering the usage of a wide collection of the novel materials or enhancing and/or modifying the performance of some existing ones like TiO₂ and ferrites. In this chapter, different composites/heterostructures based on these photocatalysts, which are employed for water splitting, are presented.

2 Semiconductor Photocatalysis

In accordance with the molecular orbitals theory, the electronic orbitals of a semiconductor are merged and split in two bands, which are separated by an energy bandgap (E_g) as shown in Fig. 3. The valance band (VB) that is created from the highest occupied molecular orbitals (HOMO) is completely filled with electrons at 0 K. In opposition, no electrons are located in the conduction band (CB), which is built from the lowest unoccupied molecular orbitals (LUMO). Hence, such an electronic band structure offers light-induced properties for semiconductors. These involve exciting the VB electrons to partially filled CB states upon absorption of appropriate light energy [11, 89]. The family of semiconductors includes various binary compounds, but not all are used for heterogeneous photocatalysis. Several criteria should be met for these binary compounds for such applications, including the right band gap energy for effective light absorption (1–4 eV), charge carrier mobility, non-toxic properties, and the positions of their band edges, which should be suitable for the particular application [112]. Most compounds and composites that work as photocatalysts are based on d-transition-metal metal oxides such as titanium dioxide (TiO₂), zinc oxide (ZnO), tungsten oxide (WO₃), and iron oxide (Fe₂O₃) [13, 67, 135]. An electron vacancy called a positively charged hole is produced in the VB after the excitation of an electron to the CB due to the illumination of the semiconductor [9, 160]. Both electrons and holes in the CB and VB, respectively, are considered mobile entities, but due to the higher diffusion coefficients of electrons, they create an electric field that pulls them back to recombine with the slower holes [134]. However, the trapping of the electrons drastically diminishes their mobilities. The charge carriers created by the light move to reach the surface due to the near-surface electric field, then the e^-/h^+ species react with adsorbed molecules. On the surface, the holes act as oxidants (+1.0 to +3.5 V vs. NHE), while electrons are consumed in reduction reactions (+0.5 to –1.5 V vs. NHE) [61]. As illustrated in Fig. 4, one of the main limitations is the recombination of charge carriers in an indirect way via surface defects (5), or through a direct band-to-band recombination (6) [28, 113]. The crystal structure of the semiconductor is the key factor affecting this

limitation. Consequently, the movement of the charge carriers to the liquid junction is essential, where the photocatalytic redox reactions with solution species on the surface take place [51]. Therefore, careful synthesis of the photocatalyst should be conducted to overcome such undesired critical issues.

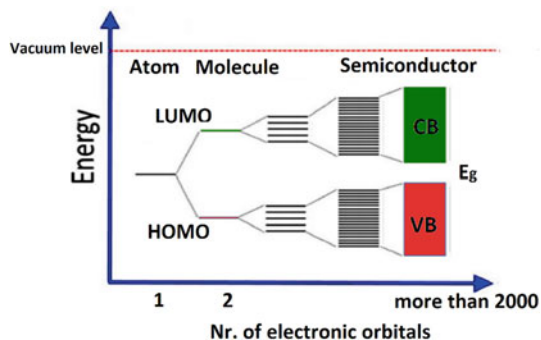


Fig. 3 Band structure of a semiconducting material based on atomic orbitals theory, adapted from the author dissertation [11]

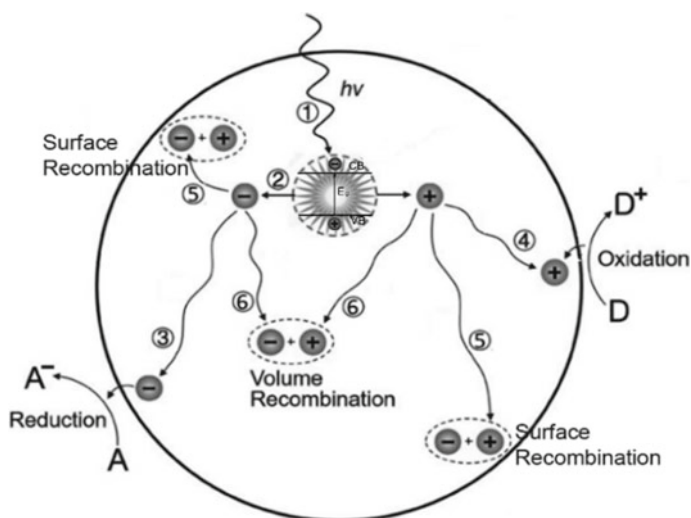


Fig. 4 Semiconducting-based photocatalyst: the possible paths of the photogenerated charge carriers, adopted with permission from ACS [102]

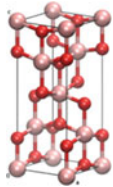
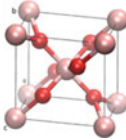
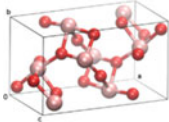
3 Titanium Dioxide Photocatalyst

Titanium dioxide (TiO₂) is a widely studied material for photocatalytic purposes since its reasonable reactivity, hydrophilic properties, high resistance to photo corrosion, and optimal electronic and optical capacity [15, 56, 62]. TiO₂ is considered as an intrinsic n-type semiconductor, in which one Ti⁴⁺ and six O²⁻ are coordinated to produce a TiO₆ octahedron [113]. TiO₂ belongs to the nonstoichiometric transition metal oxides due to the presence of oxygen vacancies as defects at ambient condition. These vacancies produce an excess of electrons, increasing the electrical conductivity [51]. Thus, the surface of n-type TiO₂ contains a lot of oxygen vacancies (O_v) defects as unpaired electrons in the CB [39, 147]. These donor-like defects lead to a downward band bending due to the creation of an accumulation layer on the surface [11, 46]. It is crucial to study the charge carrier dynamics in TiO₂ because the fast recombination of the photogenerated e⁻/h⁺ is a decisive factor that determines the competence of using TiO₂ in photocatalytic applications.

TiO₂ has three polymorphs: (1) brookite with an orthorhombic crystal structure and E_g of 3.3 eV, (2) anatase with a tetragonal crystal structure and E_g of 3.2 eV, and (3) rutile with a tetragonal crystal structure and E_g of 3.0 eV [28]. Therefore, the photocatalytic properties of all TiO₂ polymorphs are originated from the photogeneration of charge carriers after the excitation with UV irradiation. Table 1 presents the main properties of TiO₂ polymorphs. Various TiO₂ sources are available, but Degussa P25 is known as a standard photocatalytic material due to its well-defined structure containing anatase and rutile in a 3:1 ratio [56]. The thermodynamic stability of TiO₂ is highly related to the crystalline phase with its particle size. The highest thermodynamic stability can be achieved when the particle size is less than 11 nm for anatase, while it should be greater than 35 nm for rutile and lie between 11 and 35 nm for brookite [50]. TiO₂ in the anatase phase is considered commonly more active than rutile TiO₂ [7, 147]. Compared with rutile, anatase nanoparticles have relatively a higher surface area and more concentration of oxygen vacancies (O_vs), enhancing charge separation efficiency [11]. Anatase TiO₂ offers additionally a slightly higher redox capability than rutile due to its larger bandgap energy.

The synthesis of TiO₂ nanostructures with different morphologies has recently attracted great attention [121]. In this regard, TiO₂ can be fabricated as spheres [20, 171, 186], fibers [36, 181, 185], tubes [83, 105, 114], nanorods [40, 127, 181], sheets [19, 82, 151], and interconnected architectures [1, 63, 163] (see Fig. 5). Many factors largely affect the photocatalytic performance of TiO₂, e.g., particle size, pore volume, surface area, and surface facets. Therefore, regulating these factors is relevant for improving the photocatalytic performance of TiO₂. Structural dimension is also a crucial factor that gives TiO₂ different properties. While a sphere structure with zero dimension has a high surface area and high adsorption properties [103], one-dimensional fibers or tubes offer lower recombination rates due to the short distance for charge carrier diffusion [83]. On the other hand, two-dimensional nanosheets display smooth surfaces and high adhesion properties [82], while three-dimensional monoliths are characterized by their high carrier mobility due to the interconnecting

Table 1.1 Different TiO₂ polymorphs and their physicochemical properties. Data are adopted from Refs. [28, 113]

Property	Anatase TiO ₂	Rutile TiO ₂	Brookite TiO ₂
Crystal structure	Tetragonal	Tetragonal	Orthorhombic
			
Molecules/cell	4	2	8
Crystal size (nm)	<11	>35	11–35
Lattice parameters (nm)	a = b = 0.3785, c = 0.9514	a = b = 0.4594, c = 0.2959	a = c = 0.5436, b = 0.9166
Space group	<i>I</i> 4 ₁ /amd	<i>P</i> 4 ₂ /mnm	Pbca
Volume/molecule (Å ³)	34.061	31.2160	32.172
Density (g cm ⁻³)	3.79	4.13	3.99
Bandgap (eV)	3.26	3.05	3.3
dielectric constant $\xi(0)$	6.04	6.62	7.89

structure. Therefore, synthesizing TiO₂ with adequate dimensionality is very important as it may be reflected in better physicochemical and photocatalytic properties. The size can affect the efficiency of the photocatalytic system. Smaller nanoparticles are generally more suitable for photocatalytic water-splitting. In fact, the smaller size diminishes the distance of the charge carriers' migration to the surface leading to boosting the photocatalytic activity [81]. On the other hand, larger particles can be generally used for photoelectrochemical water-splitting due to the lower electron–hole recombination rate [137]. However, the recombination rate is related to the particle size, wherein in larger particles, the travel distance to the surface is longer, rising the likelihood of electron–hole recombination [50, 91].

TiO₂ is photoexcited and generates charge carriers within a few femtoseconds. Thereafter, these charge carriers either recombine with each other (in the bulk and/or at the surface) or move to the surface of TiO₂ for trapping or for initiating interfacial redox reactions [140]. Therefore, the photocatalytic efficiency of TiO₂ is related to the competition between charge carrier recombination, charge carrier trapping, and interfacial charge transfer [69]. It has been proven, that the quantum yield of photooxidation using TiO₂ in aqueous media is lower than 10% because more than 90% of the photogenerated charge carriers tend to recombine within 10 ns after UV irradiation [149]. However, the size of TiO₂ nanoparticles plays a crucial role, where 10–30 nm particle size is optimal for photocatalysis [24, 29] because of the

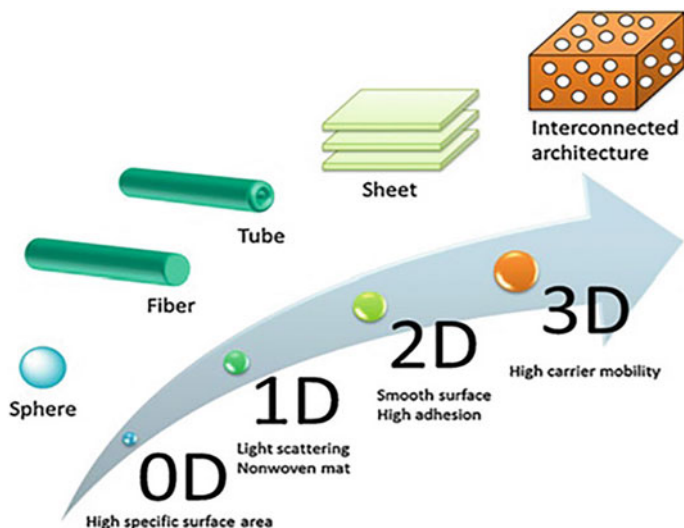


Fig. 5 Scheme of the material's structural dimensionality and their properties with permission from Elsevier [121]

faster migration and trapping of the charge carriers in the small particles. In contrast, the photogenerated e^-/h^+ can be trapped as trapped holes, trapped electrons in the bulk or at the surface or they can remain as free electrons distributed in the bulk [179]. Finally, e^-/h^+ pairs can induce a water-splitting reaction through an interfacial charge carrier transfer. Nevertheless, the incompatibility between very short lifetimes of e^-/h^+ pairs and slower kinetics of redox reactions is the main drawback in TiO₂ photocatalysis [54].

4 Synthesis of TiO₂ Photocatalytic Nanoparticles

Many synthesis procedures with diverse parameters have been successfully applied for the synthesis of TiO₂ photocatalysts. These include sol–gel, surfactant-based micelle, hydrothermal, solvothermal, chemical or physical vapor deposition, sonochemical, and microwave methods. A wide range of titanium precursors has been also applied, including titanium chloride, titanium sulfate, and titanium alkoxides. Nevertheless, the choice of the synthesis procedure in addition to the precursor type and the parameters applied has a pronounced impact on the structural, electronic, and optical properties of the synthesized TiO₂ nanoparticles [14, 176].

Nanostructured TiO₂ spheres are typically synthesized using titanium alkoxide precursors such as titanium tetra-isopropoxide or titanium tetra-butoxide. While adding an acid would accelerate the synthesis procedure, the existence of a polymer offers a porous assembly [103]. Further treatment using the hydrothermal method

has been shown to produce porous or hierarchical structures. TiO₂ photocatalysts that have a one-dimensional structure in form of fibers and tubes have demonstrated a higher surface-to-volume ratio, allowing a decrease in the hole–electron recombination rate and an increase in interfacial charge carrier transfer rate [10]. One of the various methods used for making TiO₂ fibers is the electrospinning process using a high-voltage electric field (Ramakrishna). TiO₂ fibers can be tailored in terms of diameters and morphologies by regulating the synthesis parameters, including the ratio (titanium alkoxide: polymer), the concentration of the titanium precursors, the type and molecular weight of the polymer, the solvent and electric field used, and the deposition distance [121].

Mesoporous and nanoporous TiO₂ nanoparticles have been synthesized either with or without employing organic surfactant templates [15, 33]. Such porous materials have shown a larger surface area and continuous particle frameworks, offering more active sites for the adsorption of molecules and facilitating the electron transfer within the material [103]. Evaporation-Induced Self-Assembly (EISA) is one effective method of mesoporous TiO₂ synthesis. In this method, multiple titanium precursors can be used in addition to a co-polymer surfactant molecule in an alcoholic medium to form colloidal particles before the aggregation as a three-dimensional open network. The pores are then formed upon the removal of surfactant by a calcination step [11, 33].

During water-splitting, the photogenerated charge carriers can rapidly recombine unless adequately controlled. Extensive efforts have been applied including the tuning of crystal structure, defects states, dopants, and electronic structure. However, the one-dimensional photocatalytic systems still experience from a relatively low photocatalytic activity. Alternatively, 2D photocatalytic materials can be a promising strategy because the transit distance of the photogenerated e⁻/h⁺ is relatively shorter. Two-dimensional TiO₂ nanosheets are nanosized flake-shaped materials, having a flat surface, a high aspect ratio, and a very small thickness of 1–10 nm. Such a shape is typically prepared through an alkaline hydrothermal process starting either from TiO₂ powder [152] or from protonic titanate hydrates [151].

4.1 Synthesis of Defective TiO₂ Photocatalytic Nanoparticles

Black TiO₂ have lately been suggested as a potential photocatalyst for solar-driven photocatalytic hydrogen production. Lots of efforts have been made to synthesize extremely reduced TiO₂, however, even the moderate reduction degree of TiO₂, i.e., gray TiO₂, can generate peculiar defective catalytic sites, which offer the capability to use such defective materials for cocatalyst-free hydrogen production. Nevertheless, further investigations should be carried out to understand the electronic structure of defective TiO₂ and the associated mechanisms and properties, including better light absorption and enhanced charge separation. Reduced TiO₂ can be synthesized by introducing intrinsic oxygen vacancies (VOs) and generating lattice Ti³⁺ centers. Several synthesis procedures are proposed that are typically preceded by reducing

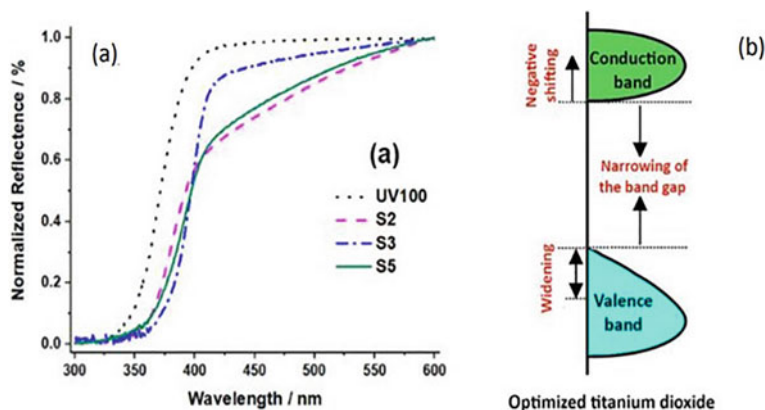


Fig. 6 UV-Visible light reflectance spectra of the prepared TiO₂ (a), schematic illustration of the band alignment (b). Adapted with permission from Elsevier [15]

TiO₂ at a high temperature using various reducing atmospheres (e.g., under vacuum, Argon, H₂/Argon mixture, and pure H₂) [31, 123]. Using such synthesis methods, gray, blue, brown, or black Ti₂O can be produced. It was found that the color obtained is related to the concentration of Ti³⁺ and VOs in the material, i.e., a strong reduction condition leads to a higher density of these defects, hence, a darker color of TiO₂ powders. The first black TiO₂ nanomaterial for photocatalysis was reported with high visible light absorption in 2011 upon thermal treatment of anatase TiO₂ at 200 °C under high pressure of H₂ (see Fig. 6a). Such an increase in the absorption of light is related to introducing electronic states and the tailing of VB and CB due to the creation of lattice disorder and H-doping (Fig. 6b) [34].

Different types of defects can be introduced that regulate many physical properties of crystalline TiO₂. Therefore, defects engineering is essential in controlling electronic, optical, and quantum properties of TiO₂, in addition to their role in the activation of TiO₂ photocatalytic processes [97]. In this regard, the synthesis method and its parameters play an essential role. As an example, the use of TiCl₃ as a precursor in the Evaporation-Induced Self-Assembly (EISA) method produced a defective TiO₂ for co-catalyst-free photocatalytic H₂ development [15]. TiCl₃ in addition to F-108 as a surfactant producing pure anatase TiO₂ that is characterized by its response to the visible region as shown in Fig. 6a. The unique photocatalytic activity of bare TiO₂ in the reforming of ethanol to generate hydrogen gas was explained by an increased carrier density alongside the extension of the edge of VB and the shift in the CB edge potential (see Fig. 6b).

The crystal defects can be generally classified regarding their dimensionalities [123, 132]. Zero-dimensional (0D) defects (point defects) are generated from a single or a few atomic positions (Fig. 7a). Such point defects can be found as Ti vacancy Ti^V (rare), Ti interstitial Tiⁱ (common), Oxygen vacancy VO (common in reduced TiO₂), and interstitial (e.g., hydrogen or nonmetal dopants) or substitutional impurity (e.g., metal or nonmetal dopants). Upon the introduction of crystal point

defects, structural rearrangements would be initiated, leading to significant distortions in the local symmetry of Ti octahedra. This effect can, in his turn, affect the transportation and the recombination of the photogenerated charge carriers. Doping of TiO₂ by metals or the introduction of high VOs concentration contributes to additional 3d states forming below the CB [122]. However, excess electronic states below the CB can act as recombination centers for photogenerated charge carriers, lowering the photocatalytic efficiency. On the other hand, Doping of TiO₂ by nonmetal (e.g., N, C, S) and interstitials (e.g., H or Ti) creates electronic features above the VB, providing an efficient strategy to modify TiO₂ [32, 122] (Wang et al. 2017).

Another dimensional-defect type is the linear or 1D defects (dislocations), in which the crystallographic registry is lost [123]. Such types of defects lead to a lattice strain, which can be useful for TiO₂ photocatalytic activity. Otherwise, 2D crystal defects can be classified into three groups: (1) free surfaces with uncoordinated atoms, (2) interphases within a crystal such as stacking faults and antiphase boundaries, and (3) grain boundaries and two-phase boundaries (interphases). Such 2D defects are important in TiO₂ photocatalysis because they tune its surface reactivity and participate in charge transport and separation in the bulk as in the case of anatase/rutile nano-junctions [133].

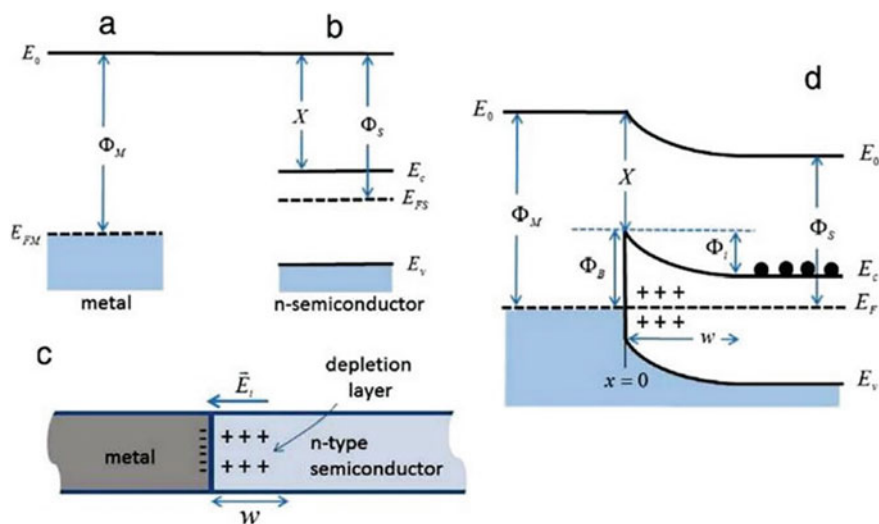


Fig. 7 A schematic represents the Schottky barrier (Sb) formation between a metal co-catalyst and n-type semiconductor. **a** Φ_M : Metal-work function and E_{FM} : Fermi level energy. **b** Φ_S : Semiconductor-work function, X : electron affinity, and E_{FS} : Fermi energy. **c** Charge distribution at the metal/semiconductor (M/S) junction. **d** M/S junction equilibrium-band-diagram. Φ_i is the energy barrier to the flow of electrons from the S to M, while Φ_B is the Sb. W is the extension of the depletion-layer. Reprinted with permission from Elsevier [45]

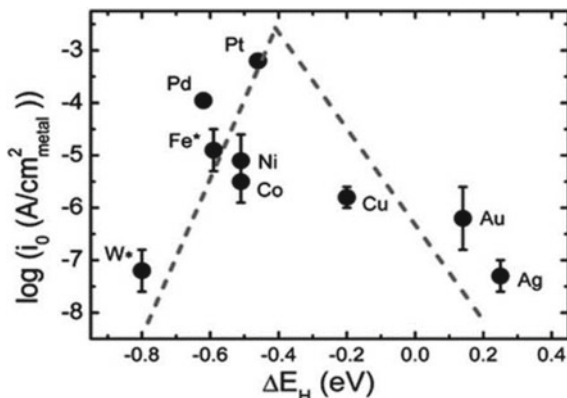
5 Modification of TiO₂

It is well known that the bandgap of the photocatalyst is the essential feature for its application in the reaction of water-splitting. Light harvesting governs electron and hole generation rates, recombination, and surface reaction kinetics. Regarding the TiO₂, the anatase, and rutile, the generally accepted bandgap values are 3.2 and 3.0, respectively [46]. While anatase is excited at 388 nm by UV light, the rutile extends slightly into the visible region at 415 nm, which can be related to the various positions of the CB and VB of both phases. The CB and VB of anatase are -0.5 V and 2.7 V, respectively, while for rutile they are -0.7 V and 2.33 V [2, 35, 146]. As mentioned in the previous section, however, TiO₂ satisfies the criterion for water-splitting, it suffers from (i) the rapid recombination between the electron-hole, where only $\sim 10\%$ of the photogenerated charge carriers successfully transfer to the interface to participate in the redox reactions which results in decreasing the reaction efficiency [147]. (ii) its large overpotential for H₂ production in water in the presence and absence of the hole scavenger. Therefore, to extend the charge carrier lifetimes, lower the overpotential of H₂ generation, and broaden the light absorption of TiO₂ towards visible light, several strategies and modifications have been employed for the TiO₂ to achieve hydrogen production from the photooxidation of water during the photocatalytic process, such as deposit metal nanoparticles like Pt, Cu, Ag, and Au on the surface of TiO₂, doping with cation or anion or sensitizing with dyes or small bandgap semiconductors.

5.1 Metal Co-Catalyst

The deposited metal co-catalyst or combination of two, such as Pd, Pt, Au, Cu, and Ag, on the surface of the semiconductor function as electrons sink that significantly reduce the recombination between the photogenerated e^-/h^+ and facilitate the reduction of water by lowering the activation energy (Yang et al. 2013). The H₂ production efficiency of different metal co-catalysts is affected by the work function of each metal. In fact, the work function of each metal plays the main role in the formation of the Schottky barrier [45]. Metal nanoparticles such as Pt (5.65 eV) and Au (5.10 eV) have higher Fermi level energy [111] compared to that TiO₂ (4.2 eV) [172]. Therefore, the photogenerated electrons move from the semiconductor to the metal nanoparticles through the interface until a thermodynamic equilibrium takes place (Fig. 7a–d) [147]. During the illumination, this equilibrium will be unsettled, thus, the generated electrons move continuously from the conduction band of the TiO₂ to the metal co-catalyst [75, 147]. The formed Schottky barrier Φ_B blocks the flow of collected electrons from the metal to the TiO₂ photocatalyst which provides an efficient separation for the charge carriers. Therefore, the trapped electrons have a longer lifetime to stimulate the reduction reactions [174, 175]. In this sense, it is worth mentioning that not all the photogenerated electrons trapping by the metal

Fig. 8 Exchange current densities, $\log(i_0)$ vs the calculated hydrogen binding energy. Reprinted with permission from Ref. [150]. Copyright 2013 from the Royal Society of Chemistry



co-catalyst. By the mean of the EPR techniques, Al-Madanat et al. showed that the irradiated Pt/TiO₂ exhibited a simultaneous signal for the Ti³⁺ centers, confirming that not all the photogenerated electrons transferred to the Pt NPs [8].

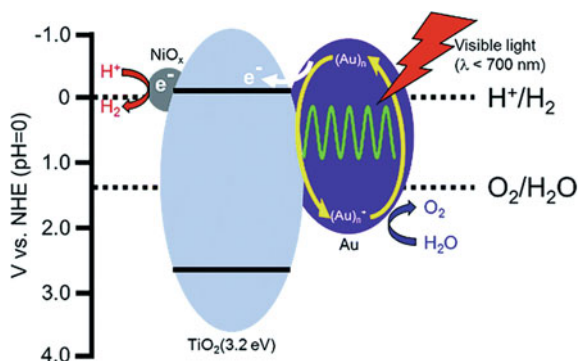
As shown in Fig. 8, Pt appears as the most active noble metal for H₂ formation [150]. Despite this general conclusion, the efficiency of H₂ production is strongly dependent on its nature, preparation method, and concentration [8, 37]. Recently, it has been shown that the preparation method used for the metal co-catalyst deposition has a strong effect on the H₂ formation during the photocatalytic reforming of naphthalene and methanol [8].

There are different common techniques used for deposition the metal co-catalyst nanoparticles on the TiO₂ nanoparticles surface including a chemical reduction [124, 167], impregnation [53], deposition–precipitation [21], photodeposition [5, 6, 12, 14, 21, 53], electrode-position [80], and physical mixing [21]. The strong interaction between the metal co-catalyst and the photocatalyst is considered the key role to ensure the electron transfer from the photocatalyst to metal efficiently, otherwise increasing the electron/hole recombination rate and decreasing the H₂ formation rate. In fact, several factors are highlighted in the literature which are associated with such methods, thus, affecting their effectiveness, such as, the weak interaction between the co-catalyst and semiconductor, the large size of the metal co-catalyst nanoparticles, and the nucleation of the isolated metallic nanoparticles in the electrolyte [115, 124, 182].

Although some researchers reported the efficiency of the bare TiO₂ (anatase) toward the H₂ production, others reported the contrary. The Photocatalytic H₂ production over co-catalyst-free TiO₂ synthesized by a simple Evaporation-Induced Self Assembly (EISA) method was achieved during the photocatalytic reforming of ethanol and oxalic acid [5, 14]. While, after loading the TiO₂ with Pt and/or Au as a co-catalyst, the authors found that the activity of the H₂ production was markedly boosted. Pt/TiO₂ exhibits greater photonic efficiencies compared to Au/TiO₂, whereas Au–Pt/TiO₂ did not show any additional advantage [12]. On contrary, other research groups proposed that bimetallic co-catalyst such as Pt–Au

and Pt–Ag shows a better activity towards H₂ production reaction with respect to the monometallic co-catalyst [78, 156]. On the contrary, when the bare Sachtleben Hombikat UV100 (TiO₂, anatase) and bare Aeroxide P25 (anatase/rutile mixture) were used as a photocatalyst during the photocatalytic reforming of methanol and naphthalene, the H₂ formation was not observed [5, 8]. However, loading these photocatalysts with Pt nanoparticles lead to photocatalyzed the proton to molecular H₂. The difference between both cases can be related to differences in the titanium-precursor type and the preparation method of the TiO₂ which leads to the formation high number of trapped states, that are advantageous for the photocatalytic properties and facilitated the H₂ production. Modification of the TiO₂ photocatalyst with copper (Cu), silver (Ag), and gold (Au) metal co-catalyst Nanoparticles is another important aspect from a practical point of view, because these metals extend the TiO₂ absorption to longer wavelengths (visible light) due to surface plasmon resonance (SPR). Several reports have shown that the irradiation of the Au/TiO₂ photocatalyst with visible light ($\lambda \geq 550$ nm) leads to the transfer of the electron from the Au nanoparticles to the semiconductor due to SPR [57, 157, 158]. Tanaka et al., discovered that plasmonic Au nanoparticles on TiO₂ act as a visible light driven photocatalyst for overall water-splitting in the absence of any additives [161]. Modification of the Au/TiO₂ with various types of metal co-catalyst nanoparticles boosted the H₂ and O₂ formation. Of these metals nanoparticles, Ni-modified Au/TiO₂ revealed 5-times higher rates of overall water splitting. This study showed that the authors designed and fabrication an effective novel solar energy conversion system consisting of three elemental technologies, including, (i) light harvesting with charge carrier separation and an active site for O₂ evolution (plasmonic Au particles). (ii) Electrons transfer from metallic Au nanoparticles to the active site to enable molecular hydrogen production (TiO₂), and (iii) Ni co-catalyst as an active site for hydrogen production (Fig. 9). In the other hand, the unfavorable reverse reaction between the molecular hydrogen and molecular oxygen into water could be suppressed by using NiOx.

Fig. 9 Photocatalytic water-splitting over an Au/TiO₂–NiOx. Reprinted from Ref. [161] with permission from the Royal Society of Chemistry



5.2 Cation or Anion Doping

In the late 1980s, other approaches have been adopted to develop second-generation TiO_2 that extend the TiO_2 visible light response, thereby enhancing the overall efficiency, by the replacement of cations or anions in the lattice. The cations (metal ions) replacement creates impurity energy levels within the bandgap of the TiO_2 , thus, facilitating the absorption in the visible range. Although a cation-doped TiO_2 can bridge both the UV and the visible radiation, it is mostly acted either as a centers for recombination of the photogenerated e^-/h^+ or ineffective in driving the surface redox reactions [148]. Moreover, the levels of impurity created by dopants in the TiO_2 photocatalysts are usually discrete, which would seem disadvantageous for the transfer of the photogenerated holes [94].

In the early 1990s, the first study of anion-doped TiO_2 was reported. However, it's reported in science published in 2001 by Asahi and co-workers that documented the preparation of the visible-light-active N-doped TiO_2 in heterogeneous photocatalysis. Afterward, several studies reported other visible-light-active materials such as C-doped TiO_2 , and S-doped TiO_2 [148]. Asahi et al. [119] reported that the doping with Nitrogen increased the photocatalytic activity of the TiO_2 in the visible light region, which shifts the absorption edge of $\text{TiO}_2\text{-xN}_x$ to lower energies through narrowing of the TiO_2 bandgap. Carbon- and sulfur-doped TiO_2 showed similar redshifts of the absorption edges and increased photoactivity [41, 180]. Different scenarios of the modifications that might occur to the TiO_2 bandgap (Fig. 10a) after doping with non-metals were presented in Fig. 10b–e.

By oxidizing titanium nitride under ambient conditions, a different kinds of N-doped TiO_2 nanostructured photocatalysts were prepared at different temperatures. N- TiO_2 calcined at 450 °C manifested the highest H_2 evolution activity in comparison to the other synthesized and commercial materials under UV–Vis illumination. The highest H_2 activity of the N-doped photocatalyst was attributed to the bandgap energy shifting toward the visible region [184].

Besides, loading the metal ion and the metal oxide on the surface of N-doped TiO_2 leads to enhancing the photocatalytic activity toward the production of hydrogen [49, 99]. Lin et al. [101] synthesized M–N/ TiO_2 (M: Cr, Ni, Cu, Nb) by using the microwave-assisted method. These materials exhibit a higher photocatalytic molecular hydrogen production activity than the N doped TiO_2 and the pristine TiO_2 . Among all the prepared doped TiO_2 photocatalysts, Cu–N/ TiO_2 showed the highest activity due to the synergistic effects of Cu and N that leading to formation an impurity energy levels which decreases bandgap energy and enhances the charge separation.

5.3 Dye Sensitizing

Another effective strategy to enhance the photoactivity of the wide bandgap semiconductor by harvesting the visible light is dye sensitizing. in this technique, the

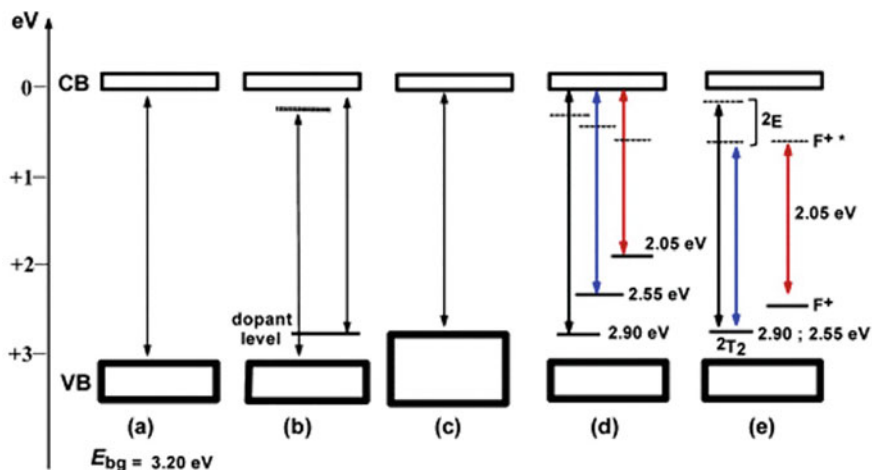


Fig. 10 Possible modification to anatase TiO₂ photocatalyst electronic structure after doping with different nonmetals: **a** pristine TiO₂; **b** localized dopant levels near the valence and conduction band of TiO₂; **c** expanding the valence band for TiO₂ narrowed the bandgap; **d** localized dopant levels and electronic transitions to the conduction band of the TiO₂; and **e** electronic transitions from localized levels near the valence band to their corresponding excited states for Ti³⁺ and F⁺ centers. With permission from ACS [148]

dye sensitizer acts as an energy antenna and does not change the properties of the semiconductor. The physical principle of the dye's sensitization process is based on the excitation of dye as a result to the absorption of light with suitable energy. This process is resulted to inject the electrons from the excited state of the dye into the CB of the semiconductor. In order for this process to take place, the excited state of the dye should possess a higher energy than the photocatalyst CB. In this case, the VB of the semiconductor remains unaffected in this process, whilst the CB acts as a mediator for transferring the excited electrons from the sensitizer to the electron acceptors on the surface of the photocatalyst [91]. Despite that various attempts have been done to enhance the photocatalytic activity of water-splitting, the production of molecular hydrogen and molecular oxygen in a single dye-sensitized system is still far away from the lowest accepted level (5%) of solar-to-H₂ conversion efficiency, which is represent 30% in terms of a quantum yield at 600 nm as suggested by Kudo [91]. The one-step excitation of Ru(bpy)₃²⁺·C₁₂-sensitized Pt/TiO₂/RuO₂ exhibits a quantum yield of ~5% under λ > 400 nm light irradiation [183].

The photocatalytic efficiency of molecular hydrogen production from splitting the water can be improved in the dye-sensitized semiconductor suspension systems by loading the semiconductor with a metal co-catalyst and using a sacrificial electron donor in this system [35, 162]. It was reported that thiophenothiazine@Pt/TiO₂ showed a reliable performance for molecular hydrogen

production from water-splitting at neutral conditions. The (E)-3-(10-hexyl-8-(methylthio)-10H-phenothiazin-3-yl)-2-cyanoacrylic acid sensitized Pt/TiO₂ photocatalyst exhibited up to 1048 μmol H₂ evolution with an apparent quantum yield around 50% [162].

6 Introduction to Ferrites

Ferrites are the most earth abundant minerals. They are promising candidate as photocatalysts due to their small band gaps and interesting magnetic properties. Most ferrites have a typical formulation of AB₂O₄, as shown in Fig. 11a. Oxygen ions are positioned in cubic closed packing, tetrahedral sites, A, and octahedral sites, B, are taken by metal cations. Such structure offers various combinations of metal cations that could show different properties. A is a transition metal and could be any of the transition metals like, Mg, Co, Mn, Ni, Cu or Zn. There is deficiency in abundance of some metals like Bi and Te making it difficult to meet large scale energy demand. On the other hand, many of the important indispensable elements used to in ferrites synthesis are abundant in earth's crust [168, 178]. Thus, earth abundance is an important factor to consider which will be reflected on the price of the metals, as presented in Fig. 11b. However, some rare earth elements frequently utilized in catalysis, like Platinum (Pt), Iridium (Ir), Ruthenium (Ru), and Rhodium (Rh), are less abundant and pose concern when large scale hydrogen generation and /or photocatalysis are intended.

7 Synthesis of Ferrites

Bulk ferrites are conventionally made by solid-state reaction. Such reaction consists of a series of thermal treatments with intermediary regrinding of stoichiometric admixtures of pulverized oxide precursors. Despite being cheap and could be easily scaled up, it has its own drawbacks, like the high synthesis temperatures that result in poly dispersed particles and less control over morphology. This is detrimental for most applications including photocatalytic water splitting. Dimension transformation of ferrites from bulk to nanometric scale could be realized by many different approaches; physical and chemical. Most of the physical synthesis is a “top-down” approach in which bulk pure powder is transformed into nanoscale via ball milling. It is an easy, scalable, and cost-effective technique; however, contamination is one of its biggest concerns. Conversely, chemical processes are a “bottom-up” approach where nano scale particles are synthesized through reactions of reactive species.

Many advantages are offered by the wet chemical synthesis routes, they provide better control over size, dispersibility, and morphology. Ferrites surface offer great versatility for ligand functionalization because of their high reactivity which specifies the best use. These characteristics are essential in defining the magnetism of the

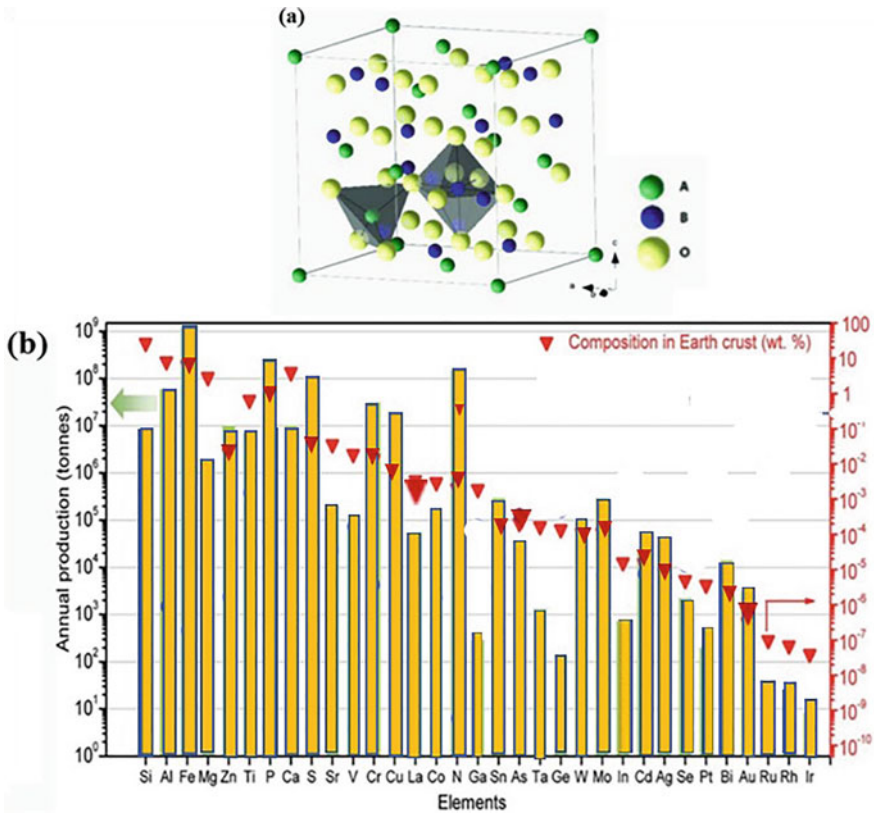


Fig. 11 a The crystal structure of ferrite AB₂O₄. b Production and inferred value data of some elements in 2010

synthesized ferrites, hence their potential applications in photocatalysis (Mendoza et al. 2016) [159], MRI [93, 131], ferrofluid [18, 141], hyperthermia and magnetic storage media [173]. Solution based chemical synthesis produce good quality ferrites with good crystallinity even though synthesized at relatively low temperature.

7.1 Co-Precipitation Method

Coprecipitation is the most popular synthetic approach used; it is straightforward, effective, and could be expanded for many of the ferrites [3, 145, 177]. It was first developed by Massart in 1981 [109]. Massart developed a method for peptizing magnetite in either alkaline or acidic media to form stable aqueous magnetic sols. It was a breakthrough such that an aqueous mixture of ferric and ferrous ions is added to the ammonia solution hence precipitates are formed. The gelatinous precipitate was

then isolated from the solution by centrifugation. In case of alkaline sol: ferrofluid is done by peptizing the precipitate with 1 molar of tetramethylammonium hydroxide aqueous solution. In case of acidic sols: precipitate is mixed with 2 molars aqueous perchloric acid, which is separated by centrifugation. Precursors used in this method are mostly inorganic divalent metal, such as sulfate, and the trivalent iron salt that are dissolved in water or any other suitable medium to form a homogeneous solution. Variety of different compositions of ferrites nanoparticles like ternary metal oxides having the nominal composition of AFe_2O_4 , where A could be Mn^{2+} , Fe^{2+} , Co^{2+} , Cu^{2+} , Zn^{2+} , [30, 58, 60, 154]. Hsu et al. [71] have been prepared using coprecipitation. In this process, the aqueous solutions containing divalent metal precursors, and trivalent iron salt mixed in proper stoichiometry are treated with a precipitating alkaline agent like NaOH, KOH, ammonia solution, or urea [26, 92] to increase the pH. Amorphous intermediates like hydroxides or oxyhydroxides are precipitated at room temperature and in a subsequent step crystallized by thermal treatment to obtain ferrites nanoparticles.

Changing experimental conditions such as the pH of the medium, reaction time and temperature, as well as the ionic strength of the used metal precursors, it is likely to acquire array of particle dimensions, phases, as well as different shapes [107, 108, 143]. Figure 12a shows the crystal structure of Mn ferrite synthesized by coprecipitation method. One can clearly see the evolving of the XRD peaks with the change in pH. XRD of $MnFe_2O_4$ synthesized at pH = 9.0 displays broad and low strength peaks indicating small-scale particles and little crystallinity. Increasing the pH value up to 10.5 results in sharp and more intense peaks, indicating higher crystallinity and larger particle size. As expected, the surface area (BET measurements) shown in Fig. 12b, of $MnFe_2O_4$ corresponds well with the induced size changes. Measured surface area values were $182.82 \text{ m}^2 \text{ g}^{-1}$ and $53.99 \text{ m}^2 \text{ g}^{-1}$ at pH 9.0 and 10.5, respectively. The observed decrease in surface area at pH 10.5 is related to the accumulation of small particles into larger ones. The average pore diameter, as seen from the BET measurements, increased as the pH increased and are shown in Fig. 12c. It was also reported that saturation magnetization, M_s , of the Manganese ferrite nanoparticles enhanced with the increase in the pH. At the pH value of 10.5, the recorded value of M_s is 41.48 emu g^{-1} owing to the large magnetic dipole moments of the particles. One important disadvantage of the coprecipitation method is the difficulties of complete separation of nucleation process from growth stages, that eventually contribute to the wide-ranging size distribution observed. In these cases, the resulting nano powder should be thermally annealed to enhance crystallinity and related properties like magnetization [3, 177].

7.2 Sol Gel Method

Sol Gel is a well known preparation technique that is widely used for the preparation of several types of materials like magnetic [16, 84, 87, 88, 139], ferroelectric [23, 66] and thermomechanics [52], multiferroics as well as glasses [43] and catalysts [72,

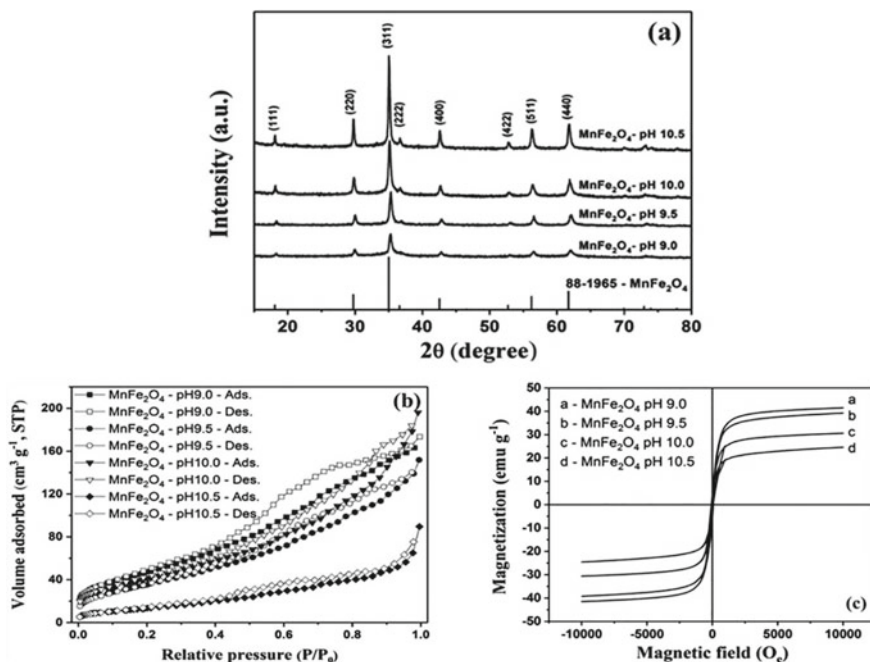


Fig. 12 a XRD patterns of MnFe₂O₄ synthesized by coprecipitation. b N₂ adsorption–desorption isotherms at different pH. c Magnetization of MnFe₂O₄ synthesized at various pH. With permission from RSC

164]. The emergence of sol gel process was in the year 1921, and 40 years later, in the 1960s. It was further developed and promoted due to the need for new synthesis techniques in the nuclear industry. Ever since flurry of research in materials science using sol gel was reported. Fundamentals of sol–gel technique require knowledge in the fields of physics (aspects related to fractal geometry and percolation theorem) and chemistry (hydrolysis and condensation) and ceramics (sintering). Sol gel is a multi-step synthetic technique that could involve a variety of precursors [65]. The most used precursors in sol gel are the alkoxides and the metal salts. Binary metal oxides having the formula M₂O_z, where M could be Ti, Zr, Nb, Ta, Ce or Th have been successfully synthesized using sol gel technique from the corresponding metal alkoxides [104, 164]. Metal salts precursors are usually used in the synthesis of complex structures like hexagonal ferrites (MFe₂O₄ and MFe₁₂O₁₉) [64, 98, 136]. Metal alkoxides are popular precursors because they react readily with water in a reaction called hydrolysis, because the hydroxyl ion becomes attached to the metal atom, as shown in the following reaction:



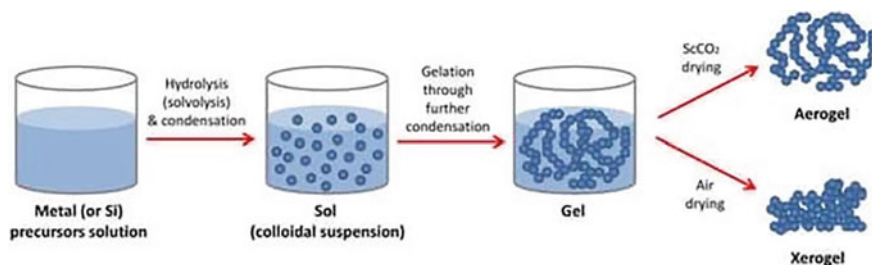


Fig. 13 Representative diagram of the Sol Gel Process. Open access from MDPI Catalysts, 2018

Here, R represents an alkyl group and ROH is alcohol. The increase in the alkyl chain length retards the hydrolysis of alkoxy silanes, while, increasing its degree of branching lowered the hydrolysis rate due to the steric effect [25]. colloid is defined as a suspension in which the dispersed phase or particles is s in the range of 1–1000 nm. In this case gravitational forces are expected to be trivial and interaction between particles is mainly governed by forces, such as van-der Waals and surface charges. TAquired inertia by scattered phase is small enough to exhibit Brownian motion. Such motion is motivated by momentum conveyed by collisions with molecules in the medium. There are two chemical processes that are commonly participating in the sol gel method: hydrolysis of the metal alkoxide used as a precursor as well as the condensation of the intermediates. Both reactions, hydrolysis, and condensation, occur either concurrently or separately. The hydrolysis reaction takes place when a proton is eliminated from the coordination sphere of the cation hence, promoting the possibility of generation of the different types of intermediates like metal hydroxo-aqua ($M(OH)_x(H_2O)_N$), metal oxyhydroxide ($MO(OH)_N$) or metal hydroxide ($M(OH)_N$) where M is the metal ion.

Condensation process liberates molecules such as water or alcohol and continues to build larger metal-containing molecules or clusters collide and link to produce giant clusters called gel. Clusters in the sol phase are mostly tangled in but not connected to the spanning cluster. However, with time, they get attached to the network causing an increase in the gel stiffness. On the other hand, the bond between clusters forming networks is responsible for the elasticity of the created solid network. Figure 13 is a graphic diagram showing the different steps of sol gel formation.

8 Water Splitting Application

Solar water splitting is one way to produce what is become known as green hydrogen. Many factors influence the performance of semiconductor materials intended to be used for hydrogen production making it a rich topic of scientific research. Finding materials with suitable properties like stability, efficient charge separation and transportation, and showing activity in the visible light region of the solar spectrum is still a

challenge [169]. In this context, ferrites can offer some of the above-mentioned properties and all of them have suitable bandgap to harvest visible light ($E_g \leq 2.6$ eV) [77]. The variety of transition elements that could fit in the composition and the multiple valency states according to the metal cation used are major factors in enhancing photocatalytic water splitting [159]. This could improve the electrical conductivity of ferrites compared to the single-component iron oxide (γ/α Fe₂O₃). This improvement is primarily ascribed to the existence of various metal cations which enable electrons transportation and/or establish rich redox chemistry [110]. Many inorganic compounds were used for photocatalytic water splitting [91, 106, 117] but metal oxides, in general, and ferrites, are considered materials of interest for water splitting due to stability under the different photocatalytic operation parameters and the facile synthesis techniques used with the ability to scale up for large scale application, unlike the organic materials. Basic properties like band position of the valence and conduction bands compared to water splitting redox potential were investigated and shown in Fig. 14. As shown in the figure, ferrites could be n-type, and p-type like p-CaFe₂O₄. They are mostly small band gaps materials which make them harvest photon in the visible range of the solar spectrum. Some of them have the suitable band positions required for full water splitting redox reactions i.e., the simultaneous generation of hydrogen and oxygen. However, and despite the many advantages, their photocatalytic performance is poor in comparison to other well-established semiconductors like TiO₂ and BiVO₄. The energy required for complete water splitting is 1.23 eV and this energy as well as the energy necessary to overwhelm the kinetic barrier of the reaction should be provided by a light absorber. Even though position of both CB and VB in some ferrites is suitable for full water splitting, it does not happen in practice. There are other factors that could be responsible for the inferior performance of ferrites like their indirect bandgap features, weak charge carrier dynamics, short diffusion lengths and short lived charges [130]. As far as we know, there are no reports of full water splitting achieved using ferrites alone in a photocatalytic process. And while bias free photocatalytic water splitting remains a significant challenge, a lot of advancement has been made, especially in the last decade, in electrically biased photoelectrodes. Formation of heterojunction and/or solid solution is another method used to achieve complete water splitting. Another adopted technique is the usage of a hole/electron scavenger that enables half-cycle water splitting i.e. production of either O₂ or H₂ [47, 117]. The usage of ferrites in photocatalytic water splitting, along with any other material, is commonly achieved by three different methods depending on their role in the photocatalytic process: they could be photo-cathodes, photo-anodes, or aqueous suspensions.

8.1 *The Effect of Cocatalyst*

There are two primary processes involved in any photocatalytic process: charge carrier separation and catalytic redox reactions on the surface. And to enhance these two processes to boost the photocatalytic water splitting performance of ferrites,

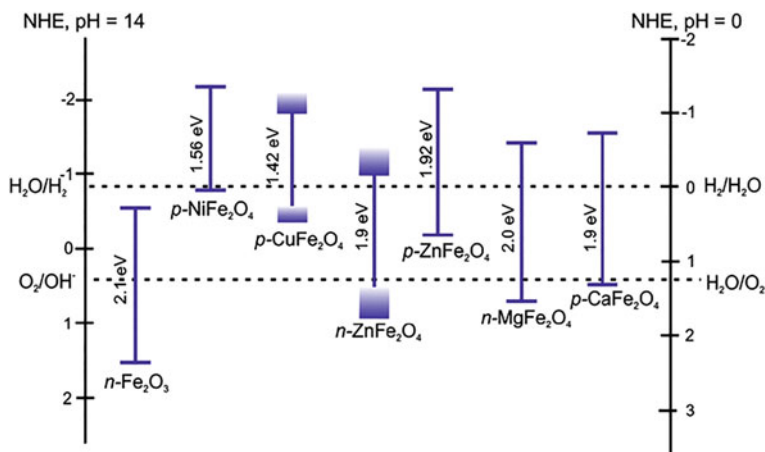
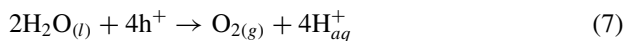


Fig. 14 Band positions of some ferrites with respect to NHE. With permission from SPIE [159]

coupling with cocatalyst seems to be a successful way to enhance charge separation [76]. Platinum (Pt) as a cocatalyst has been broadly examined and proven to be an effective cocatalyst for hydrogen evolution reaction, HER. platinum (Pt) works as a trap for electrons promoted to the surface after light irradiation thereby minimizing electrons and holes recombination, consequently enhancing the photocatalytic performance [73]. Platinum was added to magnetite, Fe_3O_4 , nanoparticles from platinum salt source like chloroplatinic acid and was deposited on the ferrite surface during a photo chemical reaction. It was reported that hydrogen amount intensely increased by Pt addition a yield of $8275 \mu\text{mol h}^{-1} \text{g}^{-1}$ compared to a yield of $458 \mu\text{mol h}^{-1} \text{g}^{-1}$ without Pt addition. The optimum amount of platinum producing the largest amount of H_2 was 0.095 mg. An increased amount of metal particles on the surface of a photocatalyst could potentially reduce the absorption of photons. Moreover, cocatalyst may function as a recombination center for the photo-generated charge carriers, thus, lowering photocatalytic performance [138]. Similar behavior was observed for bismuth ferrite, BiFeO_3 , BFO, but for oxygen evolution reaction, OER, and the usage of IrO_2 as cocatalyst [142]. OER is somehow difficult, the creation of a single molecule of oxygen involves 4holes as indicated in Eq. 7 [118]. OER occurs on a time scale approximately 5 orders of magnitude slower than H_2 evolution.



IrO_2 is one of the most active O_2 -evolution catalysts and is located on top of the volcanic catalyst diagram shown in Fig. 15a. Other oxides like NiO , RhO_2 , RuO_2 , and Co_3O_4 are also at the apex of the volcanic graph [22] and some of them are more abundant and affordable in terms of their cost compared to IrO_2 . However, IrO_2 has an important advantage over the other cocatalysts, it shows good stability

against corrosive environment which make IrO₂ more favorable in different reaction mediums [17]. The capability of a catalyst to achieve either water oxidation or reduction depends on the CB and VB position, as mentioned earlier in this chapter, which could be constructed using Mott Schottky measurements. In the case of bismuth ferrite, BFO, the CB and the VB lie at -0.46 V and 2.69 V, respectively, against NHE (Fig. 15b). It clearly shows that the bottom of the CB is more positive than the reduction potential of the proton (H⁺) to produce molecular hydrogen. But the top of the VB in BFO is also more positive than the oxidation potential of H₂O hence, it is anticipated that BFO is capable of only water oxidation (Fig. 15b). An important and facile technique to load cocatalyst oxides outside the surface of the catalyst is the impregnation method [74] in which Ir precursor in water was evaporated in a water bath, then calcined at 260 °C. In Fig. 16c, the photocatalytic oxygen evolved at different IrO₂ content is shown. Many considerations can impact the ability of OER cocatalyst activity as the type of cocatalyst and the loading amount of both the catalyst and the cocatalyst in the reaction medium. there is a bell shape type of dependance relating the amount of a cocatalyst and photo catalytic performance. Figure 15d shows the OER dependance on the loading amount of IrO₂ cocatalyst on surface of BFO, OER reaches an optimum value at 2wt % IrO₂ content. The small-scale of the cocatalyst particles makes it difficult for charge carriers to interact via recombination in the bulk of such small-scale particles. It worth mentioning here, that additional increase in the IrO₂ loading caused a reduction in the OER activity. The reduction might be related to many possibilities. The high-level of loading is likely to cover up the surface active sites on the BiFeO₃ surface preventing its interaction with the sacrificial agent and/or water. On the other hand, a high level of cocatalyst loading could reduce or at worst prevent light absorption, afterwards lower the photo-generated holes inside the BFO. One other key component influences the cocatalyst effectiveness is the cocatalyst dimension such that at greater IrO₂ loading content, cocatalyst accumulate forming separate islands on the surface of the catalyst, thus wasting the benefit of the nano length scale and the large surface area.

8.2 Ferrites Based Heterojunction

Constructing semiconducting heterojunctions was always an effective way to promote charge carriers separation. Ferrites show exciting photocatalytic and photo electrochemical properties towards water splitting application. Magnesium ferrite, MgFe₂O₄, and zinc ferrite, ZnFe₂O₄, have demonstrated ability for water oxidation reactions upon formation of CoFe₂O₃/MgFe₂O₄ and α -Fe₂O₃/ZnFe₂O₄ heterojunctions [70, 85, 86]. In such heterojunctions, the photoinduced holes are moved from the VB of semiconductors like CoFe₂O₃, and α -Fe₂O₃ to the VB of the ferrites owing to the more negative VB location of the ferrites, this in turn will lead to efficient charge carrier separation. In the same context, the semiconductor, graphitic carbon nitride (g-C₃N₄) which has narrow band gap of the order of 2.7 eV and shows

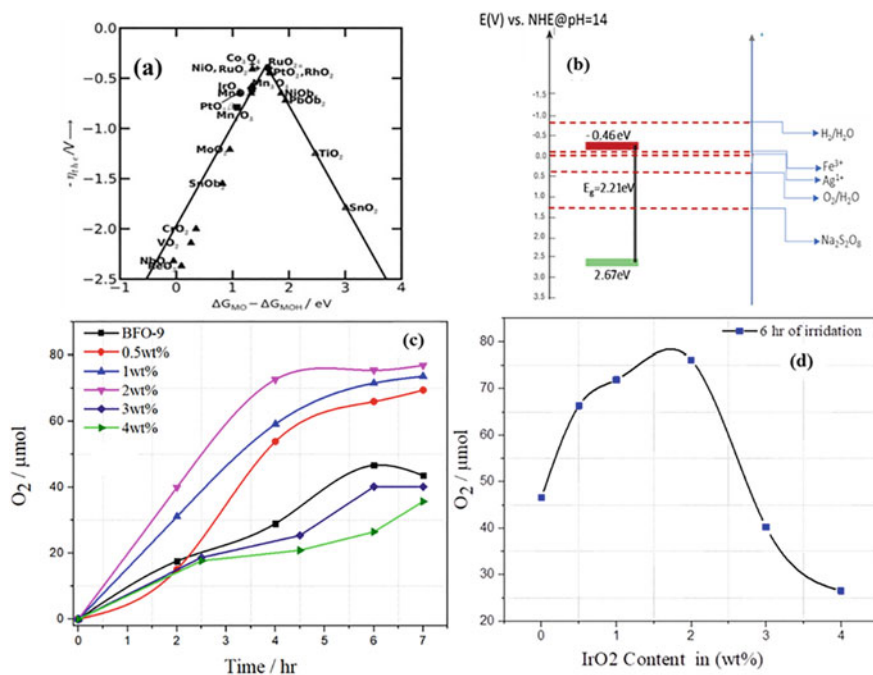


Fig. 15 a Volcano plots for the photocatalytic Oxygen Evolution Reaction (OER. With permission from RSC (Fabbri et al. 2014). b Graphic diagram showing the CB and VB in bismuth ferrite. c Photocatalytic OER at various IrO_2 cocatalyst on BFO under solar irradiation. d Relation of photocatalytic oxygen evolution of BFO/IrO_2 on the content of IrO_2 . With permission from Elsevier publisher [142]

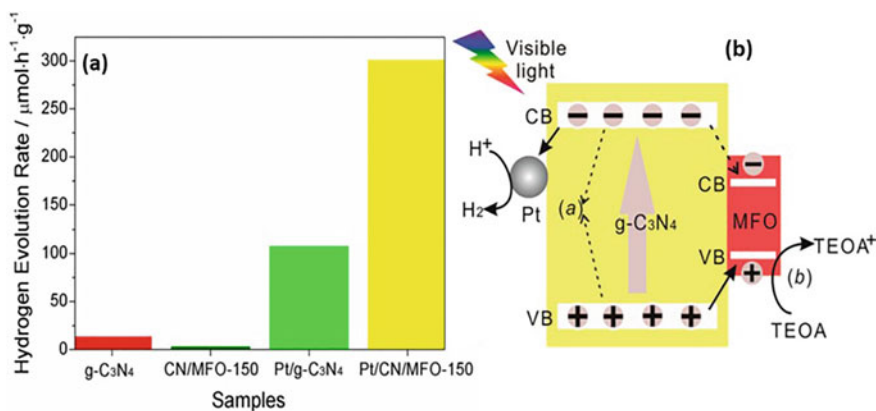


Fig. 16 a Histogram showing photocatalytic H_2 generation of graphitic carbon nitride loaded with 1 wt.% Pt cocatalyst and/or MgFe_2O_4 . b Proposed structure of the photocatalytic H_2 generation over Pt and $\text{g-C}_3\text{N}_4/\text{MgFe}_2\text{O}_4$ Heterojunction with permission from ACS publisher [34]

suitable band positions, versus NHE. such properties making it a favorable material to produce both H₂ and O₂. However, both g-C₃N₄ and MgFe₂O₄ show poor responses toward photocatalytic H₂ production (Fig. 16a). Chen and coworker [31] used a heterojunction of MgFe₂O₄ ferrite and g-C₃N₄ and assessed their performance for H₂ production. However, the photocatalytic activity of gC₃N₄/MgFe₂O₄ is quite poor, which could be explained by taking the band position of g-C₃N₄ and MgFe₂O₄ into consideration. The bandgaps (E_g) of g-C₃N₄ and MgFe₂O₄ were calculated from the UV–Vis measurements and concluded to be 2.68 and 1.78 eV, respectively.

The VB maximum location of both magnesium ferrite and graphitic carbon nitride are 1.79 and 2.39 eV, respectively. In the same way, the CB maximum of both compounds are 0.01 eV, lower than fermi level, and 0.29 eV, over the fermi level, respectively, showing difference in the CB maxima of 0.28 eV which will assist electrons to move from the CB of g-C₃N₄ to the CB of MgFe₂O₄. On the other hand, the difference between the VB maxima of the two compounds is 0.60 eV which will encourage hole transport from the VB of g-C₃N₄ to the VB of MgFe₂O₄. Therefore, formation of heterostructure and the associated change in band structures of g-C₃N₄ and MgFe₂O₄ could initiate movement of photoinduced electrons and holes from g-C₃N₄ to MgFe₂O₄. However, such charge allocation in the heterojunction will promote charge carrier recombination at MgFe₂O₄, thus and again, weak photocatalytic activity of the proposed junction. The photoinduced charge carriers in the proposed heterojunction chosed to move to the magnesium ferrite, MgFe₂O₄, unfortunately, it was unable of photocatalytic H₂ generation. Therefore, the resolve to a good H₂ catalyst like Pt to boost H₂ production. The proposed mechanism in this approach for hydrogen production over Pt loading on g-C₃N₄/MgFe₂O₄ heterojunction is shown in Fig. 16b. To establish high photocatalytic activity, photogenerated electrons in g-C₃N₄ should be confined in their position meanwhile, holes continued in transferring from g-C₃N₄ to MgFe₂O₄. By using Pt, which is a good hydrogen catalyst, electrons could be entrapped in the g-C₃N₄ and could not migrate into the ferrite, hence promote charge separation and induce efficient photocatalytic activity towards H₂ production. One can conclude that the charge transport procedures in the Pt/g-C₃N₄/MgFe₂O₄ are quite distinct from those in g-C₃N₄/MgFe₂O₄. The photoinduced electrons in g-C₃N₄ prefer to move to the metal Pt for H₂ creation instead of being exhausted at the ferrite, MgFe₂O₄, in the Pt/g-C₃N₄/MgFe₂O₄. Pt as a reductive hydrogen production catalyst is essential in this case and in many similar cases.

9 Concluding Remarks

This chapter covered some aspects of the most used synthesis techniques for TiO₂ and ferrites nano-structures and their application in photocatalytic water splitting towards H₂ production. Choice of the synthesis procedures in addition to the precursor's type and the applied parameters have a great influence on the structural, electronic, and optical characteristics of the synthesized nanoparticles. Mesoporous and nanoporous nanoparticles also demonstrate a larger surface area and continuous particle frameworks, offering more active sites for the adsorption of molecules, and facilitating the electron transfer within the material. In photocatalytic water-splitting, the photo-generated charge carriers can rapidly recombine unless controlled. In this regard, synthesis techniques including the tuning of crystal structure, defects states under inert atmosphere, dopants, and electronic structure can influence the H₂ production. Synthesis and application are two synchronized processes in these two materials as well other most systems. Meanwhile, TiO₂ is a well-established photocatalyst with good photocatalytic water splitting, ferrites in its pure form, and despite the many advantages they can offer, have poor photocatalytic performance, and can perform better with the application of biased voltage, formation of heterojunction with other semiconductors to adjust bands position and/or the attachment of cocatalyst on the surface.

Acknowledgements Some of the studies presented here were performed in the laboratory “Photoactive nanocomposite materials” and supported by Saint-Petersburg State University (ID: 91696387). Wegdan Ramadan, would like to acknowledge fund received from the Alexander von Humboldt Foundation towards the purchase of laboratory equipment.

References

1. Ahn SH, Koh JH, Seo JA, Kim JH (2010) Structure control of organized mesoporous TiO₂ films templated by graft copolymers for dye -sensitized solar cells. *Chem Commun* 46(11):1935–1937
2. AL-Azri ZHN, Chen W-T, Chan A, Jovic V, Ina T, Idriss H, Waterhouse GIN (2015) The roles of metal co-catalysts and reaction media in photocatalytic hydrogen production: performance evaluation of M/TiO₂ photocatalysts (M=Pt, Au) in different alcohol–water mixtures. *J Catal* 329:355–367
3. Albuquerque AS, Tolentino MVC, Ardisson JD, Moura FCC, De Mendona R, MacEdo WAA (2012) Nanostructured ferrites: structural analysis and catalytic activity. *Ceram Int* 38(3):2225–2231
4. Al-Madanat O (2021) Photocatalytic transformation of water pollutants into fuels. Doctoral thesis, Gottfried Wilhelm Leibniz Universität Hannover, Germany
5. A-Madanat O, AlSalka Y, Curti M, Dillert R, Bahnemann DW (2020) Mechanistic insights into hydrogen evolution by photocatalytic reforming of naphthalene. *ACS Catal* 10(13):7398–7412
6. A-Madanat O, AlSalka Y, Dillert R, Bahnemann DW (2021a) Photocatalytic H₂ production from naphthalene by various TiO₂ photocatalysts: impact of Pt loading and formation of intermediates. *Catalysts* 11(1):107

7. A-Madanat O, AlSalka Y, Ramadan W, Bahnemann DW (2021b) TiO₂ photocatalysis for the transformation of aromatic water pollutants into fuels. *Catalysts* 11(3):317
8. A-Madanat O, Curti M, Günnemann C, AlSalka Y, Dillert R, Bahnemann DW (2021c) TiO₂ photocatalysis: impact of the platinum loading method on reductive and oxidative half-reactions. *Catal Today* 380:3–15
9. Al-Madanat O, Nunes BN, AlSalka Y, Hakki A, Curti M, Patrocínio AOT, Bahnemann DW (2021d) Application of EPR spectroscopy in TiO₂ and Nb₂O₅ photocatalysis. *Catalysts* 11:1514
10. Almquist CB, Biswas P (2002) Role of synthesis method and particle size of nanostructured TiO₂ on its photoactivity. *J Catal* 212(2):145–156
11. AlSalka Y (2020) Photocatalytic water splitting for solar hydrogen production and simultaneous decontamination of organic pollutants. Doctoral thesis, Gottfried Wilhelm Leibniz Universität
12. AlSalka Y, Al-Madanat O, Curti M, Hakki A, Bahnemann DW (2020) Photocatalytic H₂ evolution from oxalic acid: Effect of cocatalysts and carbon dioxide radical anion on the surface charge transfer mechanisms. *ACS Appl Energy Mater* 3(7):6678–6691
13. AlSalka Y, Granone LI, Ramadan W, Hakki A, Dillert R, Bahnemann DW (2019) Iron-based photocatalytic and photoelectrocatalytic nano-structures: facts, perspectives, and expectations. *Appl Catal B* 244:1065–1095
14. AlSalka Y, Hakki A, Fleisch M, Bahnemann DW (2018) Understanding the degradation pathways of oxalic acid in different photocatalytic systems: towards simultaneous photocatalytic hydrogen evolution. *J Photochem Photobiol, A* 366:81–90
15. AlSalka Y, Hakki A, Schneider J, Bahnemann DW (2018) Co-catalyst-free photocatalytic hydrogen evolution on TiO₂: synthesis of optimized photocatalyst through statistical material science. *Appl Catal B* 238:422–433
16. An SY, Shim I-B, Kim CS (2002) Mössbauer and magnetic properties of Co–Ti substituted barium hexaferrite nanoparticles. *J Appl Phys* 91(10):8465
17. Harriman A, Pickering I, Thomas J (1988) Metal oxides as heterogeneous catalysts for oxygen evolution under photochemical conditions. *J Chem Soc Faraday Trans 1*(84):2795–2806
18. Anton AIJ (1990) Measurements of turbulence suppression due to a transverse magnetic field applied on a ferrofluid motion. *J Magn Magn Mater* 85:137
19. Aoyama Y, Oaki Y, Ise R, Imai H (2012) Mesocrystal nanosheet of rutile TiO₂ and its reaction selectivity as a photocatalyst. *Cryst Eng Comm* 14(4):1405–1411
20. Bai H, Liu Z, Sun DD (2010) Hierarchically multifunctional TiO₂ nano-thorn membrane for water purification. *Chem Commun* 46:6542–6544
21. Bamwenda GR, Tsubota S, Nakamura T, Haruta M (1995) Photoassisted hydrogen production from a water-ethanol solution: a comparison of activities of Au-TiO₂ and Pt-TiO₂. *J Photochem Photobiol, A* 89(2):177–189
22. Ma B, Yang J, Han H, Wang J, Zhang X, Li C (2010) Enhancement of photocatalytic water oxidation activity on IrO_x ZnO/ Zn_{2-x} GeO_{4-x}-3yN_{2y} catalyst with the solid solution phase junction. *J Phys Chem C* 114(29):12818–12822
23. Barbooram K, Ye Z-G (2006) New soft chemical routes to ferroelectric SrBi₂Ta₂O₉. *Chem Mater* 18(2):532–540
24. Bessekhoad Y, Robert D, Weber JV (2003) Synthesis of photocatalytic TiO₂ nanoparticles: optimization of the preparation conditions. *J Photochem Photobiol, A* 157(1):47–53
25. Brinker CJ (1988) Hydrolysis and condensation of silicates: effects on structure. *J Non-Cryst Solids* 100(1):31–50
26. Bruce IJ, Taylor J, Todd M, Davies MJ, Borioni E, Sangregorio C, Sen T (2004) Synthesis, characterisation and application of silica-magnetite nanocomposites. *J Magn Magn Mater* 284:145–160
27. Aydın C, Al-Hartomy O, Al-Ghamdi AA, Al-Hazmi F, Yahia IS, El-Tantawy F, Yakuphanoglu F (2012) Controlling of crystal size and optical band gap of CdO nanopowder semiconductors by low and high Fe contents. *J Electroceram* 29(2):155–162

28. Carp O, Huisman CL, Reller A (2004) Photoinduced reactivity of titanium dioxide. *Prog Solid State Chem* 32(1–2):33–177
29. Chae SY, Park MK, Lee SK, Kim TY, Kim SK, Lee WI (2003) Preparation of size controlled TiO₂ nanoparticles and derivation of optically transparent photocatalytic films. *Chem Mater* 15(17):3326–3331
30. Chen JP, Sorensen CM, Klabunde KJ, Hadjipanayis GC, Devlin E, Kostikas A (1996) Size-dependent magnetic properties of MnFe₂O₄ fine particles synthesized by coprecipitation. *Phys Rev B* 54(13):9288
31. Chen J, Zhao D, Diao Z, Wang M, Guo L, Shen S (2015) Bifunctional modification of graphitic carbon nitride with MgFe₂O₄ for enhanced photocatalytic hydrogen generation. *ACS Appl Mater Interfaces* 7(33):18843–18848
32. Chen X, Burda C (2008) The electronic origin of the visible-light absorption properties of C-, N- and S-doped TiO₂ nanomaterials. *J Am Chem Soc* 130:5018–5019
33. Chen X, Mao SS (2007) Titanium dioxide nanomaterials: synthesis, properties, modifications, and applications. *Chem Rev* 107(7):2891–2959
34. Chen X, Liu L, Huang F (2015) Black titanium dioxide (TiO₂) nanomaterials. *Chem Soc Rev* 44:1861–1885
35. Chen X, Shen S, Guo L, Mao SS (2010) Semiconductor-based photocatalytic hydrogen generation. *Chem Rev* 110(11):6503–6570
36. Cheng Y, Huang W, Zhang Y, Zhu L, Liu Y, Fan X, Cao X (2010) Preparation of TiO₂ hollow nanofibers by electrospinning combined with sol–gel process. *Cryst Eng Comm* 12(7):2256–2260
37. Chiarello GL, Forni L, Selli E (2009) Photocatalytic hydrogen production by liquid- and gas-phase reforming of CH₃OH over flame-made TiO₂ and Au/TiO₂. *Catal Today* 144(1):69–74
38. Cho S, Jang J-W, Lee K-H, Lee JS (2014) Research update: Strategies for efficient photoelectrochemical water splitting using metal oxide photoanodes. *APL Mater* 2:010703
39. Chretien S, Metiu H (2011) Electronic structure of partially reduced rutile TiO₂ (110) surface: where are the unpaired electrons located? *J Phys Chem C* 115(11):4696–4705
40. Cozzoli D, Kornowski A, Weller H (2003) Low-Temperature synthesis of soluble and processable organic-capped anatase TiO₂ nanorods. *J Am Chem Soc* 125:14539–14548
41. Damm C, Sakthivel S, Kisch H (2006) UV and visible light acrylate photopolymerisation initiated by nitrogen- or carbon-doped titanium dioxide. *Z Phys Chem* 220(4):477–486
42. Das D, Veziroglu TN (2008) Advances in biological hydrogen production processes. *Int J Hydrogen Energy* 33(21):6046–6057
43. Del Castillo J, Rodríguez VD, Yanes AC, Méndez-Ramos J, Torres ME (2005) Luminescent properties of transparent nanostructured Eu³⁺ doped SnO₂–SiO₂ glass-ceramics prepared by the sol–gel method. *Nanotechnology* 16:S300
44. Taffa D, Dillert R, Ulpe A, Bauerfeind K, Bredow T, Bahnemann DW, Wark M (2016) Photoelectrochemical and theoretical investigations of spinel type ferrites (M_xFe_{3–x}O₄) for water splitting: a mini-review. *J Photonics Energy* 7(1):012009
45. Di Bartolomeo A (2016) Graphene schottky diodes: an experimental review of the rectifying graphene/semiconductor heterojunction. *Phys Rep* 606:1–58
46. Diebold U (2003) The surface science of titanium dioxide. *Surf Sci Rep* 48(5–8):53–229
47. Dillert R, Taffa DH, Wark M, Bredow T, Bahnemann DW (2015) Research Update: Photoelectrochemical water splitting and photocatalytic hydrogen production using ferrites (MFe₂O₄) under visible light irradiation. *APL Mater* 3:104001
48. Doman L (2017) Today in energy [Online]. USA: U.S. Energy Information Administration. Available: <https://www.eia.gov/todayinenergy/detail.php?id=32912>. Accessed 08 Jan 2020
49. Du S, Lian J, Zhang F (2022) Visible light-responsive N-doped TiO₂ photocatalysis: synthesis, characterizations, and applications. *Trans Tianjin Univ* 28:33–52
50. Eidsvåg H, Bentouba S, Vajeeston P, Yohi S, Velauthapillai D (2021) TiO₂ as a photocatalyst for water splitting: an experimental and theoretical review. *Molecules* 26(6):1687
51. Enke CG (1974) Nonstoichiometry, diffusion, and electrical conductivity in binary metal oxides. *Mater Corros* 25(10):801–802

52. Fantozzi G, Chevalier J, Guilhot B (2001) Processing, microstructure, and thermomechanical behavior of ceramics. *Adv Eng Mater* 3(8):563
53. Farsinezhad S, Sharma H, Shankar K (2015) Interfacial band alignment for photocatalytic charge separation in TiO₂ nanotube arrays coated with CuPt nanoparticles. *Phys Chem Chem Phys* 17:29723–29733
54. Fazio G, Selli D, Ferraro L, Seifert G, Di Valentin C (2018) Curved TiO₂ nanoparticles in water: short (chemical) and long (physical) range interfacial effects. *ACS Appl Mater Interfaces* 10(35):29943–29953
55. Fonash SJ (2010) Chapter three: structures, materials, and scale. In: Fonash SJ (ed) *Solar cell device physics*, 2nd edn. Academic Press, Boston
56. Friehs E, AlSalka Y, Jonczyk R, Lavrentieva A, Jochums A, Walter J-G, Stahl F, Scheper T, Bahnemann DW (2016) Toxicity, phototoxicity and biocidal activity of nanoparticles employed in photocatalysis. *J Photochem Photobiol, C* 29:1–28
57. Furube A, Du L, Hara K, Katoh R, Tachiya M (2007) Ultrafast plasmon-induced electron transfer from gold nanodots into TiO₂ nanoparticles. *J Am Chem Soc* 129(48):14852–14853
58. Gee SH, Hong YK, Erickson DW, Park MH, Sur JC (2003) Synthesis and aging effect of spherical magnetite nanoparticles for biosensor applications. *J Appl Phys* 93(10):7560
59. Godula-Jopek A (2015) *Hydrogen production: by electrolysis*. Wiley-VCH, Weinheim, Germany
60. Grasset F, Labhsetwar N, Li D, Park DC, Saito N, Haneda H, Cador O, Roisnel T, Mornet S, Duguet E, Portier J, Etourneau JL, Grasset F, Labhsetwar N, Li D, Park DC, Saito N, Haneda H, Cador O, Roisnel T, Mornet S, Duguet E, Portier JE (2002) Synthesis and magnetic characterization of zinc ferrite nanoparticles with different environments: powder, colloidal solution, and zinc ferrite–silica core–shell nanoparticles. *Langmuir* 18(21):8209–8216
61. Habisreutinger SN, Schmidt-Mende L, Stolarczyk JK (2013) Photocatalytic reduction of CO₂ on TiO₂ and other semiconductors. *Angew Chem Int Ed* 52(29):7372–7408
62. Hakki A, AlSalka Y, Mendive C, Ubogui J, Dos Santos Claro P, Bahnemann DW (2018) Hydrogen production by heterogeneous photocatalysis. In: Wandelt K (ed) *Encyclopedia of interfacial chemistry*. Elsevier, Oxford
63. Hasegawa G, Morisato K, Kanamori K, Nakanishi K (2011) New hierarchically porous titania monoliths for chromatographic separation media. *J Sep Sci* 34(21):3004–3010
64. He X, Song G, Zhu J (2005) Non-stoichiometric NiZn ferrite by sol-gel processing. *Mater Lett* 59(14–15):1941–1944
65. Hench LL, West JK (1990) The sol-gel process. *Chem Rev* 90(1):33–72
66. Hernandez BA, Chang K-S, Fisher ER, Dorhout PK (2002) Sol-gel template synthesis and characterization of BaTiO₃ and PbTiO₃ nanotubes. *Chem Mater* 14(2):480–482
67. Hernández-Ramírez A, Medina-Ramírez I (2015) Semiconducting materials. In: Hernández-Ramírez A, Medina-Ramírez I (eds) *Photocatalytic semiconductors: synthesis, characterization, and environmental applications*. Springer International Publishing, Cham
68. Toulhoat H, Raybaud P (2020) Prediction of optimal catalysts for a given chemical reaction. *Catal Sci Technol* 10:2069–2081
69. Hoffmann MR, Martin ST, Choi W, Bahnemann DW (1995) Environmental applications of semiconductor photocatalysis. *Chem Rev* 95:69–96
70. Hou Y, Zuo F, Dagg A, Feng PA (2013) Three-dimensional branched cobalt-doped α -Fe₂O₃ nanorod/MgFe₂O₄ heterojunction array as a flexible photoanode for efficient photoelectrochemical water oxidation. *Angew Chem Int Ed* 52:1248–1252
71. Hsu WC, Chen SC, Kuo PC, Lie CT, Tsai WS (2004) Preparation of NiCuZn ferrite nanoparticles from chemical co-precipitation method and the magnetic properties after sintering. *Mat Sci Eng B* 111:142–149
72. Hu Q, Zhao J, Wang Y, Zhu L, Li M, Li G, Wang Y, Ge FJ (2003) Sol-gel encapsulated cobalt (III) acetylacetonate for air oxidation of penicillin derivatives. *Catal A: Chem* 200:271–277
73. Ida S, Yamada K, Matsuka M, Hagiwara H, Ishihara T (2012) Photoelectrochemical hydrogen production from water using p-type and n-type oxide semiconductor electrodes. *Electrochim Acta* 82:397–401

74. Ivanova I, Kandiel TA, Cho YJ, Choi W, Bahnemann DW (2018) Mechanisms of photocatalytic molecular hydrogen and molecular oxygen evolution over La-Doped NaTaO₃ particles: effect of different cocatalysts and their specific activity. *ACS Catal* 8:2313–2325
75. Iwata K, Takaya T, Hamaguchi H-O, Yamakata A, Ishibashi T-A, Onishi H, Kuroda H (2004) Carrier dynamics in TiO₂ and Pt/TiO₂ powders observed by femtosecond time-resolved near-infrared spectroscopy at a spectral region of 0.9– 1.5 μm with the direct absorption method. *J Phys Chem B* 108:20233–20239
76. Yang JH, Wang DE, Han HX, Li C (2013) Roles of cocatalysts in photocatalysis and photoelectrocatalysis. *Acc Chem Res* 46:1900–1909
77. Kim JH, Kim HE, Kim JH, Lee JS (2020) Ferrites: emerging light absorbers for solar water splitting. *J Mater Chem A* 8:9447–9482
78. Jiang Z, Zhu J, Liu D, Wei W, Xie J, Chen M (2014) In situ synthesis of bimetallic Ag/Pt loaded single-crystalline anatase TiO₂ hollow nano-hemispheres and their improved photocatalytic properties. *Cryst Eng Comm* 16:2384–2394
79. Kampouri S, Stylianou KC (2019) Dual-functional photocatalysis for simultaneous hydrogen production and oxidation of organic substances. *ACS Catal* 9(5):4247–4270. <https://doi.org/10.1021/acscatal.9b00332>
80. Kang J-G, Sohn Y (2011) Interfacial nature of Ag nanoparticles supported on TiO₂ photocatalysts. *J Mater Sci* 47:824–832
81. Kato H, Asakura K, Kudo A (2003) Highly efficient water splitting into H₂ and O₂ over lanthanum-doped NaTaO₃ photocatalysts with high crystallinity and surface nanostructure. *J Am Chem Soc* 125(10):3082–3089. Available from <https://doi.org/10.1021/ja027751g>
82. Katsumatak KI, Okazaki S, Cordonier CEJ, Shichi T, Sasaki T, Fujishima A (2010) Preparation and characterization of self-cleaning glass for vehicle with niobia nanosheets. *ACS Appl Mater Interfaces* 2:1236–1241
83. Kazuya N, Baoshun L, Yosuke I, Munetoshi S, Hidenori S, Tsuyoshi O, Hideki S, Taketoshi M, Masahiko A, Katsuhiko T, Akira F (2011) Fabrication and photocatalytic properties of TiO₂ nanotube arrays modified with phosphate. *Chem Lett* 40:1107–1109
84. Kim CS, Yi YS, Park K-T, Namgung H, Lee J-G (1999) Growth of ultrafine Co–Mn ferrite and magnetic properties by a sol–gel method. *J Appl Phys* 35(8):5223
85. Kim E, Nishimura N, Magesh G, Kim JY, Jang J-W, Jun H, Kubota J, Domen K, Lee JS (2013) Fabrication of CaFe₂O₄/TaON heterojunction photoanode for photoelectrochemical water oxidation. *J Am Chem Soc* 135:5375–5383
86. Kim HG, Borse PH, Jang JS, Jeong ED, Jung O-S, Suh YJ, Lee JS (2009) Fabrication of CaFe₂O₄/MgFe₂O₄ bulk heterojunction for enhanced visible light photocatalysis. *Chem Commun* 5889–5891
87. Kim WC, Kim SJ, Sur JC, Kim CS (2002) Structural and magnetic properties of CoFe_{1.9}RE_{0.1}O₄ (RE=Y, La) prepared by a sol–gel method. *J Magn Magn Mater* 242–245:197–200
88. Kim WC, Park SI, Kim SJ, Lee SW, Kim CS (2000) Magnetic and structural properties of ultrafine Ni–Zn–Cu ferrite grown by a sol–gel method. *J Appl Phys* 87(9):6241
89. Kisch H (2014) Molecular photochemistry. *Semicond Photocatalysis* 9–46
90. Kisch H (2015) Semiconductor photocatalysis principle and applications. Wiley-VCH
91. Kudo A, Miseki Y (2009) Heterogeneous photocatalyst materials for water splitting. *Chem Soc Rev* 38:253–278
92. Kundu A, Upadhyay C, Verma HC (2003) Magnetic properties of a partially inverted zinc ferrite synthesized by a new coprecipitation technique using urea. *Phys Lett A* 311:410–415
93. Lawaezck R, Menzel M, Pietsch H (2004) Superparamagnetic iron oxide particles: contrast media for magnetic resonance imaging. *Appl Organometal Chem* 18:506–513
94. Lee JS (2005) Photocatalytic water splitting under visible light with particulate semiconductor catalysts. *Catal Surv Asia* 9:217–227
95. Lee SW, Ryu YG, Yang KJ, Jung K-D, An SY, Kim CS (2002) Magnetic properties of Zn²⁺ substituted ultrafine Co-ferrite grown by a sol-gel method. *J Appl Phys* 91(10):7610

96. Lewis NS, Nocera DG (2006) Powering the planet: chemical challenges in solar energy utilization. *Proc Natl Acad Sci* 103:15729–15735
97. Li G, Blake GR, Palstra TTM (2017) Vacancies in functional materials for clean energy storage and harvesting: the perfect imperfection. *Chem Soc Rev* 46:1693–1706
98. Li J-J, Xu W, Yuan H-M, Chen J-S (2004) Sol-gel synthesis and magnetization study of Mn_{1-x}Cu_xFe₂O₄ (x=0, 0.2) nanocrystallites. *Solid State Commun* 131:519–522
99. Li Y, Peng Y-K, Hu L, Zheng J, Prabhakaran D, Wu S, Puchtler TJ, Li M, Wong K-Y, Taylor RA, Tsang SCE (2019) Photocatalytic water splitting by N-TiO₂ on MgO (111) with exceptional quantum efficiencies at elevated temperatures. *Nat Commun* 10:4421
100. Liao C-H, Huang C-W, Wu J (2012) Hydrogen production from semiconductor-based photocatalysis via water splitting. *Catalysts* 2:490–516
101. Lin HY, Shih CY (2016) Efficient one-pot microwave-assisted hydrothermal synthesis of M (M=Cr, Ni, Cu, Nb) and nitrogen co-doped TiO₂ for hydrogen production by photocatalytic water splitting. *J Mol Catal A: Chem* 411:128–137
102. Linsebiglerl A-L, Lu G, Yates JT (1995) Photocatalysis on TiO₂ surfaces: principles, mechanisms, and selected results. *Chem Rev* 95:735–758
103. Liu B, Nakata K, Sakai M, Saito H, Ochiai T, Murakami T, Takagi K, Fujishima A (2011) Mesoporous TiO₂ core-shell spheres composed of nanocrystals with exposed high-energy facets: facile synthesis and formation mechanism. *Langmuir* 27:8500–8508
104. Livage J, Henry M, Sanchez C (1988) Sol-gel chemistry of transition metal oxides. *Prog Solid St Chem* 18:259–341
105. Macak JM, Zlamal M, Krysa J, Schmuki P (2007) Self-organized TiO₂ nanotube layers as highly efficient photocatalysts. *Small* 3:300–304
106. Marschall R (2014) Semiconductor composites: strategies for enhancing charge carrier separation to improve photocatalytic activity. *Adv Funct Mater* 24(17):2421–2440
107. Mascolo M, Pei Y, Ring T (2013) Room temperature co-precipitation synthesis of magnetite nanoparticles in a large pH window with different bases. *Materials* 6(12):5549–5567
108. Massart R, Cabuil V (1987) New trends in chemistry of magnetic colloids: polar and non polar magnetic fluids, emulsions, capsules and vesicles. *J Chim Phys PCB* 84:967–973
109. Massart R (1981) Preparation of aqueous magnetic liquids in alkaline and acidic media. *IEEE Trans Magn* 17:1247–1248
110. Matsumoto Y (1996) Energy positions of oxide semiconductors and photocatalysis with iron complex oxides. *J Solid State Chem* 126(2):227–234
111. Michaelson HB (1977) The work function of the elements and its periodicity. *J Appl Phys* 48:4729–4733
112. Mills A, Le Hunte S (1997) An overview of semiconductor photocatalysis. *J Photochem Photobiol, A* 108:1–35
113. Mo SD, Ching W (1995) Electronic and optical properties of three phases of titanium dioxide: rutile, anatase, and brookite. *Phys Rev B* 51:13023
114. Mohajerina S, Mazare A, Gongadze E, Kralj-Iglič V, Iglič A, Schmuki P (2017) Self-organized, free-standing TiO₂ nanotube membranes: effect of surface electrokinetic properties on flow-through membranes. *Electrochim Acta* 245:25–31
115. Mohamed HH, Bahnemann DW (2012) The role of electron transfer in photocatalysis: fact and fictions. *Appl Catal B* 128:91–104
116. Moniz SJA (2015) Visible-light driven heterojunction photocatalysts for water splitting—a critical review. *Energy Environ Sci* 8(3):731–759
117. Moniz SJA, Shevlin SA, Martin DJ, Guo Z-X, Tang J (2015) Visible-light driven heterojunction photocatalysts for water splitting: a critical review. *Energy Environ Sci* 8:731–759
118. Moniz SJA, Quesada-Cabrera R, Blackma, Tang CS, Southern JP, Weaver PM, Carmalt CJ (2014) A simple, low-cost CVD route to thin films of BiFeO₃ for efficient water photo-oxidation. *J Mater Chem A* 2:2922–2927
119. Morikawa T, Asahi R, Ohwaki T, Aoki K, Taga Y (2001) Band-gap narrowing of titanium dioxide by nitrogen doping. *Jpn J Appl Phys* 40:L561–L563

120. Moriya Y, Takata T, Domen K (2013) Recent progress in the development of (oxy)nitride photocatalysts for water splitting under visible-light irradiation. *Coord Chem Rev* 257:1957–1969
121. Nakata K, Fujishima A (2012) TiO₂ photocatalysis: design and applications. *J Photochem Photobiol, C* 13:169–189
122. Naldoni A, Allieta M, Santangelo S, Marelli M, Fabbri F, Cappelli S, Bianchi CL, Psaro R, Dal Santo V (2012) Effect of nature and location of defects on bandgap narrowing in black TiO₂ nanoparticles. *J Am Chem Soc* 134:7600–7603
123. Naldoni A, Altomare M, Zoppellaro G, Liu N, Kment STPN, Zboril R, Schmuki P (2019) Photocatalysis with reduced TiO₂: from black TiO₂ to cocatalyst-free hydrogen production. *ACS Catal* 9:345–364
124. Naldoni A, D'Arienzo M, Altomare M, Marelli M, Scottis R, Morazzoni F, Selli E, Dal Santo V (2013) Pt and Au/TiO₂ photocatalysts for methanol reforming: Role of metal nanoparticles in tuning charge trapping properties and photoefficiency. *Appl Catal B: Environ* 130–131, 239–248
125. Avarro erga RM, Alvarez-Galvan MC, Vaquerov F, Arenales J, Fierro JLG (2013) Chapter 3—hydrogen production from water splitting using photo-semiconductor catalysts. In: Gandía LM, Arzamendi G, Diéguez PM (eds) *Renewable hydrogen technologies*. Elsevier, Amsterdam
126. Ni M, Leung MK, Leung DY, Sumathy K (2007) A review and recent developments in photocatalytic water-splitting using TiO₂ for hydrogen production. *Renew Sustain Energy Rev* 11:401–425
127. Nian J-N, Teng H (2006) Hydrothermal synthesis of single-crystalline anatase TiO₂ nanorods with nanotubes as the precursor. *J Phys Chem B* 110:4193–4198
128. Ohtani B (2010) Photocatalysis A to Z—what we know and what we do not know in a scientific sense. *J Photochem Photobiol C* 11:157–178
129. Ohtani B (2013) Titania photocatalysis beyond recombination: a critical review. *Catalysts* 3:942–953
130. Osterloh FE (2013) Inorganic nanostructures for photoelectrochemical and photocatalytic water splitting. *Chem Soc Rev* 42:2294
131. Oswald P, Clement O, Chambon C, Schouman-Claeys E, Fria G (1997) Liver positive enhancement after injection of superparamagnetic nanoparticles: respective role of circulating and uptaken particles. *Magn Reson Imaging* 15:1025–1031
132. Paul A, Lauril T, Vuorinev V, Divinski SV (2014) Structure of materials. Thermodynamics, diffusion and the Kirkendall effect in solids. Springer International Publishing, Cham
133. Penn RL, Banfield JF (1999) Formation of rutile nuclei at anatase (112) twin interfaces and the phase transformation mechanism in nanocrystalline titania. *Am Miner* 84:871–876
134. Peter LM (2016) Photoelectrochemistry: from basic principles to photocatalysis
135. Pichat P (2007) A brief overview of photocatalytic mechanisms and pathways in water. *Water Sci Technol* 55:167–173
136. Plocek J, Hutlová A, Nižňanský D, Buršík J, Rehspringer J-L, Mička Z (2003) Preparation of ZnFe₂O₄/SiO₂ and CdFe₂O₄/SiO₂ nanocomposites by sol–gel method. *J Non-Cryst Solids* 315:70–76
137. Pokrant S, Dilgre S, Landsmann S, Trotmann M (2017) Size effects of cocatalysts in photoelectrochemical and photocatalytic water splitting. *Mater Today Energy* 5:158–163
138. Mangrulkar PA, Polshettiwar V, Labhsetwar NK, Varma RS, Rayalu SS (2012) Nano-ferrites for water splitting: unprecedented high photocatalytic hydrogen production under visible light. *Nanoscale* 4:5202–5209
139. Pullar RC, Bhattacharya AK (2002) Crystallisation of hexagonal M ferrites from a stoichiometric sol-gel precursor, without formation of the α -BaFe₂O₄ intermediate phase. *Mat Lett* 57:537–542
140. Qian R, Zong H, Schneider J, Zhou G, Zhao T, Li Y, Yang J, Bahnemann DW, Pan JH (2019) Charge carrier trapping, recombination, and transfer during TiO₂ photocatalysis: an overview. *Catal Today* 335:78–90

141. Raj K, Moskovitz BC (1995) Advances in ferrofluid technology. *J Magn Magn Mater* 149:174–180
142. Ramadan W, Feldhoff A, Bahnemann D (2021) Assessing the photocatalytic oxygen evolution reaction of BiFeO₃ loaded with IrO₂ nanoparticles as cocatalyst. *Solar Energy Mater Solar Cells* 232:111349
143. Ramadan W, Kareem M, Hannover B, Saha S (2011) Effect of pH on the structural and magnetic properties of magnetite nanoparticles synthesized by co-precipitation. *Adv Mater Res* 324:129–132. Presented at the CIMA conference, Beirut-March
144. Ramakrishna S, Kazutoshik F, Teo W-E, Lim T-C, Zuwei M (2005) An introduction to electrospinning and nanofibers
145. Roonasi P, Mater NAY (2015) A comparative study of a series of ferrite nanoparticles as heterogeneous catalysts for phenol removal at neutral pH. *Chem Phys* 172:143–149
146. Scanlon DO, Dunnill CW, Buckeridge J, Shevlin SA, Logsdail AJ, Woodley SM, Catlow CRA, Powell MJ, Palgrave RG, Parkin IP, Watson GW, Keal TW, Sherwood P, Walsh A, Sokol AA (2013) Band alignment of rutile and anatase TiO₂. *Nat Mater* 12:798–801
147. Schnider J, Matsuoka M, Takeuchi M, Zhang J, Horiuchi Y, Anpo M, Bahnemann DW (2014) Understanding TiO₂ photocatalysis: mechanisms and materials. *Chem Rev* 114:9919–9986
148. Serpone N (2006) Is the band gap of pristine TiO₂ narrowed by anion- and cation-doping of titanium dioxide in second-generation photocatalysts? *J Phys Chem B* 110:24287–24293
149. Serpone N, Lawless D, Khairutdinov R (1995) Size effects on the photophysical properties of colloidal anatase TiO₂ particles: size quantization versus direct transitions in this indirect semiconductor? *J Phys Chem* 99:16646–16654
150. Sheng W, Myint M, Chen JG, Yan Y (2013) Correlating the hydrogen evolution reaction activity in alkaline electrolytes with the hydrogen binding energy on monometallic surfaces. *Energy Environ Sci* 6:1509–1512
151. Shibata T, Sakai N, Fukuda K, Ebina Y, Sasaki T (2007) Photocatalytic properties of titania nanostructured films fabricated from titania nanosheets. *Phys Chem Chem Phys* 9:2413–2420
152. Shichi T, Katsumata K-I (2010) Development of photocatalytic self-cleaning glasses utilizing metal oxide nanosheets. *Hyomen Gijutsu* 61:30–35
153. Shimura K, Yoshida H (2011) Heterogeneous photocatalytic hydrogen production from water and biomass derivatives. *Energy Environ Sci* 4:2467–2481
154. Sousa MH, Tourinho FA, Depuyot JJ, da Silva G, Lara MCFL (2001) New electric double-layered magnetic fluids based on copper, nickel, and zinc ferrite nanostructures. *J Phys Chem B* 105(6):1168–1175
155. Steinfeld A (2002) Solar hydrogen production via a two-step water-splitting thermochemical cycle based on Zn/ZnO redox reactions. *Int J Hydrogen Energy* 27:611–619
156. Su R, Forde MM, He Q, Shen Y, Wang X, Dimitratos N, Wendt S, Huang Y, Iversen BB, Kiely CJ, Besenbacher F, Hutchings GJ (2014) Well-controlled metal co-catalysts synthesised by chemical vapour impregnation for photocatalytic hydrogen production and water purification. *Dalton Trans* 43:14976–14982
157. Tada H (2019) Overall water splitting and hydrogen peroxide synthesis by gold nanoparticle-based plasmonic photocatalysts. *Nanoscale Adv* 1:4238–4245
158. Tada H (2019) Size, shape and interface control in gold nanoparticle-based plasmonic photocatalysts for solar-to-chemical transformations. *Dalton Trans* 48:6308–6313
159. Taffa Dereje H, Ralf D, Ulpe AC, Bauerfeind Katharina CL, Thomas B, Bahnemann DW, Michael W (2016) Photoelectrochemical and theoretical investigations of spinel type ferrites (M_xFe_{3-x}O₄) for water splitting: a mini-review. *J Photonics Energy* 7(1):012009
160. Takanabe K (2017) Photocatalytic water splitting: quantitative approaches toward photocatalyst by design. *ACS Catal* 7:8006–8022
161. Tanka A, Teramura K, Hosokawa S, Kominai H, Tanaka T (2017) Visible light-induced water splitting in an aqueous suspension of a plasmonic Au/TiO₂ photocatalyst with metal co-catalysts. *Chem Sci* 8:2574–2580
162. Tiwari A, Mondal I, Pal U (2015) Visible light induced hydrogen production over thiophenothiazine-based dye sensitized TiO₂ photocatalyst in neutral water. *RSC Adv* 5:31415–31421

163. Tomas SA, Zelaya O, Palomino R, Lozada R, Garcia O, Yanez JM, Ferrereira Da Silva A (2008) Optical characterization of sol gel TiO₂ monoliths doped with Brilliant Green. *Eur Phys J Special Topics* 153:255–258
164. Tseng I-H, Wu JCS, Chou H-Y (2004) Effects of sol-gel procedures on the photocatalysis of Cu/TiO₂ in CO₂ photoreduction. *J Cataly* 221:432–440
165. Walter MG, Warren EL, Mckone JR, Boettcher SW, Mi Q, Santori EA, Lewis NS (2010) Solar water splitting cells. *Chem Rev* 110:6446–6473
166. Wanf B, Shen S, Mao SS (2017) Black TiO₂ for solar hydrogen conversion. *J Materiomics* 3:96–111
167. Wang C, Yin L, Zhang L, Liu N, Lun N, Qi Y (2010) Platinum-nanoparticle-modified TiO₂ nanowires with enhanced photocatalytic property. *ACS Appl Mater Interfaces* 2:3373–3377
168. Wang Q, Domen K (2020) Particulate photocatalysts for light-driven water splitting: mechanisms, challenges, and design strategies. *Chem Rev* 120:919–985
169. Ramadan W, Dillert R, Koch J, Tegenkamp C, Bahnamn D (2019) Changes in the solid-state properties of bismuth iron oxide during the photocatalytic reformation of formic acid. *Cataly Today* 326:22–29
170. Wu L, Mendoza-Garcia A, Li Q, Sun S (2016) Organic phase syntheses of magnetic nanoparticles and their applications. *Chem Rev* 116(18):10473–10512
171. Xiang Q, Yu J, Jaroniec M (2011) Tunable photocatalytic selectivity of TiO₂ films consisted of flower-like microspheres with exposed 001 facets. *Chem Commun* 47:4532–4534
172. Xiong G, Shao R, Droubay TC, Joly AG, Beck KM, Chambers SA, Hess WP (2007) Photoemission electron microscopy of TiO₂ anatase films embedded with rutile nanocrystals. *Adv Func Mater* 17:2133–2138
173. Yamaguchi K, Matsumoto K, Fujii T (1990) Magnetic anisotropy by ferromagnetic particles alignment in a magnetic field. *J Appl Phys* 67:4493
174. Yamakata A, Ishibashi T-A, Onishi H (2001) Water-and oxygen-induced decay kinetics of photogenerated electrons in TiO₂ and Pt/TiO₂: a time-resolved infrared absorption study. *J Phys Chem B* 105:7258–7262
175. Yamakata A, Ishibashi T-A, Kato H, Kudo A, Onishi H (2003) Photodynamics of NaTaO₃ catalysts for efficient water splitting. *J Phys Chem B* 107:14383–14387
176. Yan X, Chen X (2011) Titanium dioxide nanomaterials. *Encycl Inorg Bioinorg Chem* 1–38
177. Yang L, Zhang Y, Liu X, Jiang X, Zhang Z, Zhang T, Zhang L (2014) The investigation of synergistic and competitive interaction between dye Congo red and methyl blue on magnetic MnFe₂O₄. *Chem Eng J* 246:88–96
178. Yao T, An X, Han H, Chen JQ, Li C (2018) Photo electrocatalytic materials for solar water splitting. *Adv Energy Mater* 8:1800210
179. Yoshihara T, Katoh R, Furube A, Tamaki Y, Murai M, Hara K, Murata S, Arakawa H, Tachiya M (2004) Identification of reactive species in photoexcited nanocrystalline TiO₂ films by wide-wavelength-range (400–2500 nm) transient absorption spectroscopy. *J Phys Chem B* 108:3817–3823
180. Yu JC, Ho W, Yu J, Yip H, Wong PK, Zhao J (2005) Efficient visible-light-induced photocatalytic disinfection on Sulfur-doped nanocrystalline titania. *Environ Sci Technol* 39:1175–1179
181. Yun H, Lee H, Joo J-B, Wooyoung K, Yi J (2009) Influence of aspect ratio of TiO₂ nanorods on the photocatalytic decomposition of formic acid. *J Phys Chem C J Phys Chem C* 113:3050–3055
182. Zhang L, Mohamed HH, Dillert R, Bahnamann D (2012) Kinetics and mechanisms of charge transfer processes in photocatalytic systems: a review. *J Photochem Photobiol, C* 13:263–276
183. Zhang X, Peng T, Song S (2016) Recent advances in dye-sensitized semiconductor systems for photocatalytic hydrogen production. *J Mater Chem A* 4:2365–2402
184. Zhang X, Song P, Cui X (2013) Nitrogen-doped TiO₂ photocatalysts synthesized from titanium nitride: characterizations and photocatalytic hydrogen evolution performance. *J Adv Oxid Technol* 16:131–136

185. Zhao T, Liu Z, Nakata K, Nishimoto S, Murakami T, Zhao Y, Jiang L, Fujishima A (2010) Multichannel TiO₂ hollow fibers with enhanced photocatalytic activity. *J Mater Chem* 20:5095–5099
186. Zheng Z, Huang B, Qin X, Zhang X, Dai Y (2010) Strategic synthesis of hierarchical TiO₂ microspheres with enhanced photocatalytic activity. 16:11266–11270